



Fe-N/C catalysts for oxygen reduction reaction supported on different carbonaceous materials. Performance in acidic and alkaline direct alcohol fuel cells



Luigi Osmieri ^{a,b,*}, Ricardo Escudero-Cid ^b, Marco Armandi ^a, Alessandro H.A. Monteverde Videla ^a, José Luís García Fierro ^c, Pilar Ocón ^b, Stefania Specchia ^a

^a Politecnico di Torino, Department of Applied Science and Technology, Corso Duca degli Abruzzi 24, 10129, Torino, Italy

^b Universidad Autónoma de Madrid, Departamento de Química Física Aplicada, C/Francisco Tomás y Valiente 7, 28049, Madrid, Spain

^c Grupo de Energía y Química Sostenibles, Instituto de Catálisis y Petroleoquímica, CSIC, C/Marie Curie 2, 28049, Madrid, Spain

ARTICLE INFO

Article history:

Received 25 August 2016

Received in revised form

28 December 2016

Accepted 3 January 2017

Available online 5 January 2017

Keywords:

Non-noble metal catalyst

Oxygen reduction reaction

Rotating disk electrode

Direct alcohol fuel cell

Durability

ABSTRACT

Four carbonaceous materials (acetylene black, multi-walled carbon nanotubes, and two carbon materials synthesized by hard-template method) were used as a support to synthesize four Fe-N/C non-noble metal (NNM) catalysts for oxygen reduction reaction (ORR) by impregnation with a Fe^{III}-1,10-phenanthroline complex and subsequent pyrolysis in inert atmosphere. The catalysts were characterized by N₂ physisorption, XPS, Raman and TGA, and their ORR activity was measured by rotating disk electrode (RDE) in both acidic and alkaline conditions. The catalysts were tested in an acidic direct methanol fuel cell (DMFC) and in an alkaline direct ethanol fuel cell (DEFC). Due to the slower ORR kinetics at low pH, the features of the carbon support have an important influence on the performance in acidic DMFC. Conversely, the enhanced ORR kinetics at high pH, makes the influence of the C-support less evident in alkaline DEFC. Moreover, the short-term durability test in DMFC for our best Fe-N/C catalysts showed better results compared to Pt/C benchmark catalyst. The durability in alkaline DEFC is poor, even though the initial performance can be partially recovered after purge-drying and reactivation.

© 2017 Elsevier B.V. All rights reserved.

1. Introduction

Fuel cells are devices that efficiently convert the chemical energy of a fuel into electrical energy via electrochemical reactions. Among the wide variety of fuel cell types, polymer electrolyte membrane fuel cells (PEMFC) are promising for transportation, and portable applications since they operate close to ambient conditions [1,2]. For this reason, they are key strategical components which need to be deeply investigated and furtherly developed thinking to a possible future world where clean and environmental friendly energy use and conversion will take place [3]. In particular, in direct alcohol fuel cells (DAFC), the use of a liquid

fuel (hydro-alcoholic solution) allows improving the energy density and overcoming most of the fuel storage and transportation safety issues [4]. However, the power density of DAFC is considerably lower compared to that of H₂-fueled PEMFC, due to the slow kinetics of the alcohol oxidation reaction. Therefore, their potential application is still limited to power supply units for portable and off-grid low-power devices [5,6].

Another important problem of DAFC is the fuel crossover, that is, the permeation of alcohol from the anode to the cathode through the electrolyte membrane. In fact, if Pt is used as cathodic catalyst, the fuel crossover causes the presence of a mixed potential at cathode, with a consequent considerable decrease of the fuel cell performance [7]. In addition, the use of Pt has other important drawbacks, which are its high cost and scarcity on the Earth's crust [8]. For this reason, the use of non-noble metal (NNM) catalysts, which are at the same time cheaper than Pt and methanol tolerant, is of high interest in DAFC cathode [9]. However, so far, the study of these NNM catalysts has been much more addressed to H₂-fueled PEMFC, and only few works can be found in the literature about their application in DAFC [10,11].

* Corresponding author at: Politecnico di Torino, Department of Applied Science and Technology, Corso Duca degli Abruzzi 24, 10129, Torino, Italy.

E-mail addresses: luigi.osmieri@polito.it, ligiosmi@gmail.com (L. Osmieri), ricardo.escudero@uam.es (R. Escudero-Cid), marco.armandi@polito.it (M. Armandi), alessandro.monteverdevidela@polito.it (A.H.A. Monteverde Videla), jlgfierro@icp.csic.es (J.L. García Fierro), pilar.ocon@uam.es (P. Ocón), stefania.specchia@polito.it (S. Specchia).

Direct methanol fuel cells (DMFC) are the most common and widely studied type of DAFC operating in acidic conditions. In fact, due to the simplicity of its structure (absence of C–C bonds), methanol is the alcohol which shows the faster oxidation kinetics in acidic conditions [12].

Conversely, ethanol as fuel is preferred than methanol due to its chemical and environmental safeness, as well as due to the possibility of unlimited production of ethanol from biomass. However, the existing electrocatalysts based on Pt alloy nanoparticles still lead to a very low conversion because the rupture of the C–C bond during the electro-oxidation is most likely not occurring and the complete conversion into CO₂ is very limited. In addition to this, the ethanol crossover seems to be more prominent in direct ethanol fuel cell (DEFC) than in DMFC, causing more severe losses in the performance [13].

On the other hand, more recently, DAFC operating under alkaline conditions started to attract the attention of the researchers due to the development of polymeric membranes with good anionic conductivity and durability [14,15]. In fact, operating in alkaline conditions presents several potential advantages. First, the alcohol oxidation reaction is faster than in acidic conditions [16]. Second, the ORR kinetics in alkaline conditions on several types of NNM catalysts [17] is as good as, or even better than on Pt-based catalysts, enabling an easy Pt replacement without considerable performance loss.

Moreover, the ionic current in alkaline membrane fuel cells (AMFC) has a reverse direction than in proton conducting membranes. This behavior causes a decrease in the alcohol crossover rate, because the direction of the electro-osmotic drag is reversed [5].

In the literature [18–20] the comparison of the performance between alkaline DMFC and alkaline DEFC was made under the same operative conditions, and the former was found to be much lower than the latter. The methanol could be completely oxidized to CO₂, which is prone to react with KOH and deposit causing membrane carbonation. Nonetheless, ethanol tends to be oxidized incompletely, and the C–C bond rupture is most likely not occurring avoiding the formation of CO₂. In this way, the fast membrane carbonation, which causes an irreversible decrease in the ionic conductivity, is prevented, leading to better fuel cell performance.

Among several types of NNM catalysts for ORR the most promising until now have been carbonaceous materials doped with N and transition metals (Fe, Co) [21].

To improve the activity and the stability of these catalysts, several synthesis strategies have been explored [22,23]. One of the most common approaches for the synthesis of Me-N-C NNM catalysts is the use of a carbonaceous material as a support and C source. Then, to introduce Me and N functionalities, the C-support is pyrolyzed at high temperature in the presence of N and transition metal precursors (e.g., a complex between a transition metal and a N-containing organic ligand molecule) [24–26].

1,10-phenanthroline (Phen) is a nitrogen-containing organic molecule which in water solution is capable to form complexes with Fe^{II} and Fe^{III} ions [27,28]. Due to the fact that this Fe-Phen complex contains Fe, N, and C, with nitrogen atoms coordinating the metal, it has been used as a precursor for the synthesis of heat treated non-precious metal based Fe-N-C electrocatalysts for ORR since many years [29–31]. Recently, the use of Fe-Phen complexes has aroused again the interest of researchers in the field of ORR catalysts alternative to Pt-based ones [32–35].

Several works [36–38] also pointed out the importance of using an adequate carbon support to get a good ORR activity. In particular, several types of carbon-based materials have been used as C-supports, including commercial carbon blacks (CB) [36,39], carbon nanofibers (CNF) [40], carbon nano-networks (CNN) [41], reduced

graphene oxide (rGO) [6,42,43], multi-walled carbon nanotubes (MWCNT) [25,44], and ordered mesoporous carbons (OMC) [37].

To achieve an increase of the density of the active ensembles, and assure good mass transport of reactants and products, a possible approach is to properly tune the structural features of the carbonaceous support synthesizing it using the sacrificial hard templating method [26,37,45]. Here, a sacrificial non-carbonaceous material (*i.e.*, an ordered mesoporous silica) is mixed with the C precursor and removed after the carbonization. The resulting carbonaceous material is a negative replica of the templating agent [46].

In this work, four different carbonaceous materials, that is, acetylene black (AB), MWCNT, and two different types of carbons synthesized by hard-templating method (CNS and MPC, see Section 2.2.1) were used as supports for the impregnation of the Fe^{III}-Phen complex, and subsequently pyrolyzed under inert atmosphere at 800 °C. The different catalysts were characterized by nitrogen sorption, XPS, Raman spectroscopy and TGA, and their ORR electroactivity was tested in rotating disk electrode (RDE) both in acidic and alkaline conditions. The performances of the different catalysts were finally tested in acid DMFC and in alkaline DEFC, with the purpose of pointing out how the features of the different C-supports influence the performance of each of these fuel cell types.

2. Experimental

2.1. Chemicals

Commercial multi-walled carbon nanotubes (MWCNT, average length 5 μm, outer diameter 6–9 nm, >95% carbon) were purchased from Sigma-Aldrich. Shawinigan AB50 acetylene black (AB) was purchased from Chevron Phillips Chemical Company.

Silica mesoporous nanoparticles (200 nm particle size, 4 nm pore size) and silica nanopowder (12 nm primary particle size) were purchased from Sigma-Aldrich.

Hydrochloric acid (HCl, 37 wt.%), sulfuric acid (H₂SO₄, 98 wt.%), hydrofluoric acid (HF, ≥40 wt.%), potassium hydroxide (KOH, 99.0% purity), sucrose (≥99.0% purity), ethanol (≥99.8% purity), acetone (≥99.8% purity), isopropanol (≥99.7% purity), Nafion® 5 wt.% hydro-alcoholic solution, 1,10-phenanthroline C₁₂H₈N₂ (Phen, ≥99% purity), iron(III) chloride (FeCl₃, ≥97% purity) were purchased from Sigma-Aldrich.

20 wt.% Pt/C (HiSPEC™ 3000, Pt 20 wt.% on carbon black, Johnson Matthey), 40 wt.% Pt/C (HiSPEC™ 4000, Pt 40 wt.% on carbon black, Johnson Matthey), 30 wt.% PtRu/C (HiSPEC™ 5000, Pt-Ru 30 wt.% on carbon black, Pt:Ru atomic ratio = 1, Johnson Matthey) and 45 wt.% PtRu/C (HiSPEC™ 7000, Pt-Ru 45 wt.% on carbon black, Pt:Ru atomic ratio = 1, Johnson Matthey) were purchased from Alfa Aesar.

Nitrogen and oxygen gasses were supplied in cylinders by SIAD and Air-Liquide with 99.999% purity. All aqueous solutions were prepared using ultrapure deionized water obtained from a Millipore Milli-Q system with resistivity >18 MΩ cm.

2.2. Synthesis

2.2.1. Synthesis of the carbon supports via hard-templating method

Two different carbon supports were synthesized via the hard-templating method. The templates used were the commercial silica mesoporous nanoparticles and the silica nano-powder, respectively. The synthesis method consisted in impregnating the silica with a solution containing sucrose (used as carbon source) and sulfuric acid. The impregnation was carried out in two steps, fol-

lowed by a heat treatment at 830 °C under a nitrogen atmosphere to complete the carbonization. Finally, the silica template was removed by washing with 5% wt. HF solution. The detailed procedure is described elsewhere [26,46]. The carbonaceous materials obtained from the mesoporous silica nanoparticles and the silica nano-powder were named MPC and CNS, respectively.

2.2.2. Synthesis of the Fe-N/C catalysts

Before their use, all of the C-supports (MPC, CNS, MWCNT, and AB) were washed with 1 M HCl and abundant deionized water. Four different catalysts were obtained from these C-supports, exactly following the same synthesis procedure, as described below.

Typically, for 120 mg of C-support, 130 mg of 1,10-phenanthroline (Phen) ligand molecule, used as a nitrogen source, was dissolved in 10 mL ethanol and 70 mL deionized water. Then, 35 mg of FeCl₃ was added to the solution, with the immediate formation of a red complex. According to these quantities, Fe:C-support mass ratio was 1:10, and the Fe:Phen molar ratio was of 1:3.35. Since each Fe-ion coordinates with 3 Phen molecules [27,28], the slightly greater quantity of Phen should assure a stoichiometric excess to favor the chemical equilibrium of the Fe ion complexation. Moreover, this excess of Phen (and therefore of N atoms) may help to get a higher doping level of the C-support surface with N atoms. Subsequently the C-support was added to the solution, left under stirring overnight, and the solvent was evaporated by heating on a hot plate. The recovered powder was homogenized in a mortar and pyrolyzed in a quartz tubular furnace for 1 h at 800 °C under N₂ atmosphere, with a heating ramp of 10 °C min⁻¹, according to the procedure reported in our previous work [24]. The four catalysts obtained from the different C-supports (AB, MWCNT, CNS, and MPC) were named Fe-N/AB, Fe-N/MWCNT, Fe-N/CNS, and Fe-N/MPC1, respectively.

Two selected "Fe-free" catalysts were also prepared, using the two carbon supports which showed the best and worst performance in RDE tests in both acidic and alkaline electrolyte: AB and MPC. The synthesis was carried out exactly in the same way as described above for the Fe-containing catalysts, but without the addition of FeCl₃. These two new samples were named N/AB and N/MPC, respectively.

Before testing and characterization, all of the catalysts were washed in 1 M HCl solution for 3 h at 60 °C under reflux, to remove any instable or unbounded Fe moiety [25,43,47].

For the Fe-N/MPC1, after the acid washing treatment, the pyrolysis was repeated one more time in the same conditions as the first one, and the final catalyst was named Fe-N/MPC2. Performing a second heat treatment was found to have a positive influence in improving the ORR activity for this type of Me-N-C catalysts [25,26,30,48,49].

2.3. Physicochemical characterization

2.3.1. N₂ physisorption analysis

Nitrogen adsorption and desorption isotherms of the five Fe-N/C catalysts were recorded by an ASAP 2020 Instrument (Micromeritics) at -196 °C. Before being analyzed all of the samples were degassed at 150 °C under vacuum for 24 h. The specific surface areas were calculated by the Brunauer–Emmett–Teller (BET) method in the relative pressure range 0.05–0.30 [47]. The pore size distribution was obtained with the Barrett–Joyner–Halenda (BJH) method.

2.3.2. XPS analysis

The XPS spectra of the catalysts were acquired with a VG Escalab 200R spectrometer fitted with an Mg K α ($h\nu = 1253.6$ eV) 120 W X-ray source. The samples were placed in a pretreatment chamber, and degassed at 10⁻⁵ mbar at room temperature for 1 h before being transferred to the analysis chamber. The residual pressure was

maintained below 3.0·10⁻⁸ mbar. The 50 eV energy regions of the photoelectrons of interest were scanned many times to obtain an acceptable signal-to-noise ratio. Intensities were estimated by calculating the integral of each peak, determined by subtraction of the Shirley-type background and fitting of the experimental curve to a combination of Lorentzian and Gaussian lines of variable proportions. Accurate binding energies (± 0.2 eV) were determined by referencing to the C 1s peak at 284.6 eV [50].

2.3.3. Raman spectroscopy

Raman spectroscopy was performed for all of the C-supports and for their respective Fe-N/C catalysts to evaluate the ordered/disorder degree of their carbon-based structure. The instrument used was a Raman Spectroscope (i-Raman spectrometer equipped with a Video Microscope Raman Sampling System, which includes an integrated camera and a CCD detector with an excitation wavelength of 532 nm, B&WTek Inc, USA). The light power at the exit of the laser was 150 mW and the beam was focused on the powder with a 50 \times objective. The Raman scattered light was collected in the spectral range 100–3500 cm⁻¹. For each sample, ten scans were recorded to ensure a sufficient signal to noise ratio. For the peak deconvolution analysis, in the range 800–1800 cm⁻¹, the spectra were fitted with four symmetric Lorentzian peaks.

2.3.4. TGA

Thermogravimetric analysis was performed using a TGA/SDTA 851e – Mettler Toledo analyzer under Ar flow (50 NmL min⁻¹) between 25 and 800 °C. The heating rate (10 °C min⁻¹) and dwell time (1 h) used was identical to the pyrolysis performed for the synthesis of the Fe-N/C catalysts, as described in Section 2.2.2.

2.4. RDE tests

The ORR activity of the five Fe-N/C catalysts were assessed in a 3-electrode cell using a rotating disk electrode (RRDE-3A ALS) and a multi-potentiostat (Bio-Logic SP-150). The cell was equipped with a glassy carbon disk working electrode (disk diameter 4 mm), a platinum helical wire counter electrode, and a saturated calomel reference electrode (SCE). The catalyst ink was prepared by mixing 10 mg of catalyst, 305 μ L of isopropanol, 150 μ L of deionized water and 45.8 μ L of 5% wt. Nafion[®] solution under sonication (130W, Soltec 2200M3S sonicator) for 30 min. The Nafion-to-catalyst mass ratio (NCR) is 0.2. Then, 4 μ L of ink were pipetted on the glassy carbon surface of the RDE, resulting in a catalyst load of 637 μ g cm⁻².

As a comparison, a Pt/C catalyst was also tested. The ink was prepared by dispersing 10 mg of catalyst (considering the total mass of Pt and C), 20 μ L of deionized water, 33 μ L of 5 wt.% Nafion solution and 734 μ L of isopropanol. The Pt loading on the electrode was 38 μ g cm⁻².

For the test of Fe-N/C catalysts in acidic conditions the electrolyte was a 0.5 M H₂SO₄ solution (0.1 M HClO₄ for Pt/C). In alkaline conditions the electrolyte was a 0.1 M KOH solution. Before starting tests, the electrolytes were saturated with N₂, and 50 cyclic voltammetry (CV) cycles at 100 mV s⁻¹ were performed between 0.0 and 1.2 V vs RHE. Then the solution was saturated with O₂, the RDE rotation speed was set at 900 rpm, and staircase voltammetry (SV) were recorded with a potential step of 0.01 V and a holding time at each potential of 10 s. After this time, the background capacitive current had passed, and a steady-state value of the faradaic current was measured. In this way, steady-state polarization curves were obtained [48].

2.5. Fuel cell tests

2.5.1. Acidic-DMFC test

The performance of the five different Fe-N/C catalysts at the cathode of DMFC was evaluated in a 4 cm^2 active area single cell. A commercial Nafion[®] 117 membrane (Dupont) was used as electrolyte. Before use, the membrane was treated following a procedure described elsewhere [51]. A commercial Pt-Ru/C 30 wt.% was used as an anodic catalyst. As a purpose of comparison, a DMFC with a commercial Pt/C 20 wt.% at the cathode was also evaluated.

The electrodes were prepared by spraying the catalyst ink onto a carbon cloth gas diffusion layer (ELAT GDL-LT 1200 W). The inks were prepared by mixing catalysts plus isopropanol/deionized water solution (2:1 vol.) and Nafion[®] (5 wt.%) under sonication. The Nafion[®] amount was 50 wt.% in the dry catalytic layer, and the total catalyst loading was 2.5 mg cm^{-2} . The Pt loading was 1 mg cm^{-2} in Pt-Ru and Pt-based electrodes, with a Nafion[®] content of 4 wt.% on the dry electrode.

The membrane electrode assembly (MEA) was hot pressed at 100°C and 60 bar for 3 min. A MITS Pro-FCTS, Arbin Instruments, USA was used for the evaluation. The anode was fed with 2 M methanol at a flow rate of 1 mL min^{-1} and 0.33 bar (relative). The cathode was fed with O_2 , 200 NmL min^{-1} flow rate, 3 bar backpressure and no humidification. The cell temperature was 90°C and the polarization curves were recorded at 10 mV s^{-1} from open circuit potential (E_{oc}) down to 0.0 V. A short-term durability test was also performed for the catalysts Fe-N/MPC1 and Fe-N/MPC2. It consisted in a chronoamperometric ($E = 0.4\text{ V}$, $t = 3\text{ h}$) in the same operating conditions described above, but with a methanol solution flow rate of 5 mL min^{-1} , and recording a polarization curve every 30 min, as described in our previous works [52].

2.5.2. Alkaline-DEFC test

All of the Fe-N/C catalysts were also tested in an alkaline DEFC. The single cell active area was 4 cm^2 . A commercial polybenzimidazole (PBI) membrane (Danish Power Systems) was used as electrolyte. The membrane was doped with OH^- functionalities during 7 days into 6 M KOH solution. After this treatment, the membrane ionic conductivity was around 0.01 S cm^{-1} [48].

A commercial Pt-Ru/C 45 wt.% was used at the anode catalyst. As a comparison, a commercial Pt/C catalyst (40 wt.% Pt/C) at the cathode was also evaluated. The five different Fe-N/C cathodes as well as the Pt/C one, were prepared as described for acid DMFC test. For the Pt-Ru anode the Pt loading was 1.33 mg cm^{-2} with a Nafion[®] content on the dry electrode of 4 wt.%. The electrodes and the membrane were assembled without hot pressing, by direct sandwiching in the cell hardware. The anode was fed with a 2 M ethanol and 2 M KOH solution preheated at 80°C with a flow rate of 1 mL min^{-1} and a pressure of 0.33 bar (relative). The cathode was fed with a 200 NmL min^{-1} pure O_2 flow with no humidification at 3 bar backpressure [53]. The temperature of the cell was 90°C during the experiments, and the polarization curves were recorded as described for acid DMFC test.

3. Results and discussion

3.1. Physicochemical characterization

Fig. 1a and b show the adsorption-desorption isotherms and the BJH desorption pore-size distribution of all of the Fe-N/C catalysts, respectively. Table 1 lists the BET specific surface areas and the BJH total pore volume and average pore diameter. As evident, the structure of the final catalyst strongly depends on the C-supports, which are very different from each other.

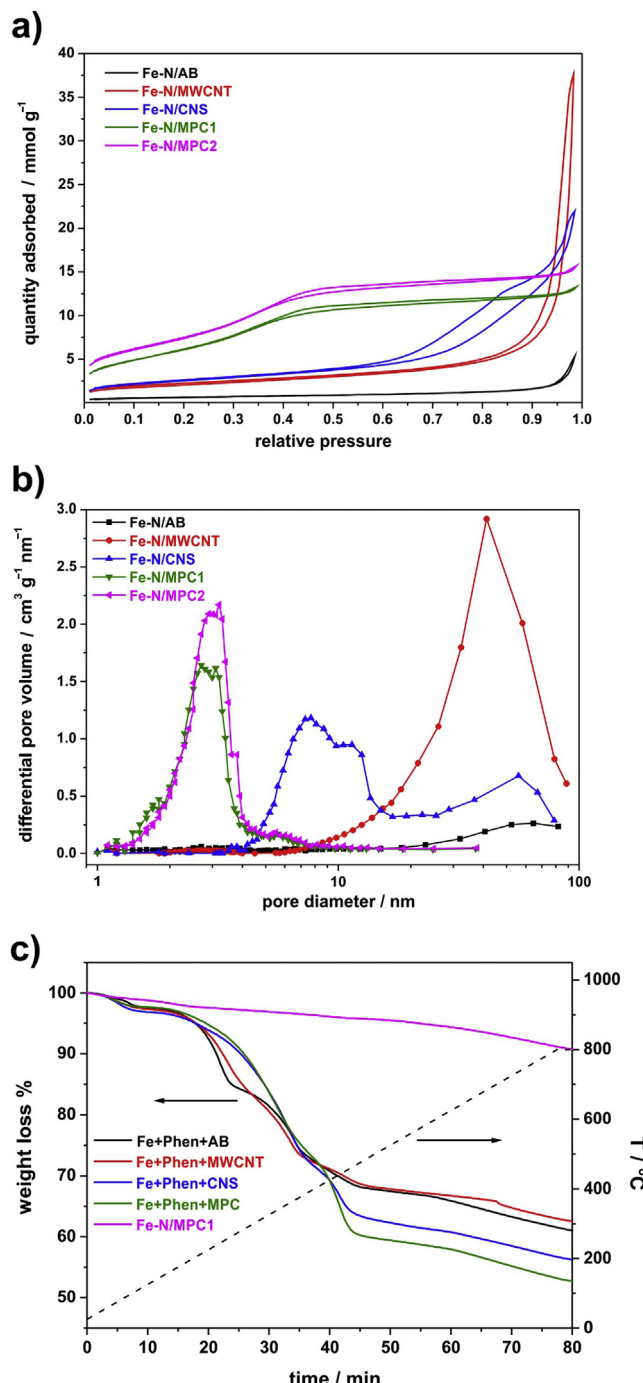


Fig. 1. (a) N₂ adsorption – desorption isotherms and (b) BJH desorption pore-size distribution of the Fe-N/C catalysts. (c) TGA curves simulating the pyrolysis of the precursors of the five different Fe-N/C catalysts.

Fe-N/AB and Fe-N/MWCNT have a strong macroporous character, as suggested by the shapes of their isotherms, which belong to type II of the IUPAC classification. At relative pressure values lower than 0.05, the shape of the isotherms suggests the presence of a low quantity of micropores [54,55]. For Fe-N/AB, there is almost no hysteresis loop. On the contrary, Fe-N/MWCNT exhibits a hysteresis loop with almost vertical adsorption and desorption branches, which are nearly parallel over an appreciable range of quantity of gas adsorbed. This hysteresis loop is typical of porous materials consisting of agglomerates [54], and can be associated with carbon nanotubes aggregates felt-like morphology [25,56].

Table 1

Properties calculated from the nitrogen physisorption analysis of the different Fe-N/C catalysts and their respective C-supports materials.

Sample	BET area [m ² g ⁻¹]	BJH total pore volume [cm ³ g ⁻¹]	BJH average pore diameter [nm]
AB	80	0.28	13.1
MWCNT	259	2.89	37.3
CNS	332	1.38	14.2
MPC	865	0.83	3.3
Fe-N/AB	51	0.17	10.8
Fe-N/MWCNT	165	1.29	31.1
Fe-N/CNS	208	0.75	11.7
Fe-N/MPC1	543	0.46	2.8
Fe-N/MPC2	645	0.55	2.9

Table 2

Overall surface elemental composition of the different Fe-N/C catalysts determined by XPS analysis.

Catalyst	C [at.%]	O [at.%]	N [at.%]	Fe [at.%]	Tot [at.%]	Fe/N
Fe-N/AB	91.9	4.5	3.3	0.3	100.0	0.09
Fe-N/MWCNT	95.3	2.5	2.1	0.1	100.0	0.05
Fe-N/CNS	91.8	5.2	2.8	0.2	100.0	0.07
Fe-N/MPC1	92.6	5.3	1.8	0.3	100.0	0.17
Fe-N/MPC2	95.1	3.1	1.5	0.3	100.0	0.20

The isotherm shape of Fe-N/CNS is an intermediate between type II and type IV, showing capillary condensation at $P/P^0 > 0.6$ and an evident hysteresis loop.

The Fe-N/MPC1 and Fe-N/MPC2 catalysts have an identical isotherm shape, with the latter showing higher quantities of adsorbed gas, due to its higher specific surface area. The shape of the isotherms belongs to type IV(b), showing capillary condensation in the 0.3–0.4 P/P^0 range due to the presence of narrow mesopores, and limited H4 hysteresis loop closing at the cavitation induced P/P^0 , as commonly observed with micro-mesoporous carbons. As shown by the pore size distribution analysis in Fig. 1b, the majority of the pores in the Fe-N/MPC1 and Fe-N/MPC2 catalysts are between 2 and 4 nm.

The results of the pore size distribution (Fig. 1b) confirm the previous considerations. In fact, it is evident that the catalysts prepared using MWCNT and AB supports mainly contain macropores and mesopores with diameter >20 nm. Fe-N/CNS catalyst exhibits a broad pores size distribution ranging from meso to macropores, with a maximum between 5 and 20 nm, having also a certain amounts of macropores. Finally, the porosity of the catalysts supported onto MPC is mainly due to narrow mesopores with a diameter between 2 and 4 nm.

The specific surface area decrease for all of the Fe-N/C catalysts is almost the same, in comparison with their respective supports. In fact, it is around 63%, being 63.7% – 63.7% – 62.6% – 62.8% for Fe-N/AB, Fe-N/MWCNT, Fe-N/CNS and Fe-N/MPC1, respectively. This fact could indicate that the Fe-Phen complex undergoes to a similar incorporation on the C-support during the heat treatment, leading to the same overall surface area% decrease, regardless of the type of C-support.

The XPS analysis was performed for all of the Fe-N/C catalysts after the final acid leaching in 1 M HCl, to determine surface chemical composition (Table 2). As expected, for all of the catalysts the main component is C, which is always detected in quantities higher than 90 atomic%. A not negligible amount of O was also detected in all of the catalysts. However, for Fe-N/MPC1 and Fe-N/CNS the amount of O was higher than in the other catalysts. This could be due to the not complete carbonization of the sucrose during the synthesis of MPC and CNS supports. For the Fe-N/MPC2 catalyst (that is, the Fe-N/MPC1 after a second heat treatment at 800 °C in inert atmosphere), the O content was lower (3.1 at.%), suggesting that during the second heat treatment the surface of the catalyst

undergoes to the loss of some oxidized functional groups. The O content in the catalysts synthesized using the commercial supports (MWCNT and AB) is lower. However, the presence of O has to be ascribed to the carbonaceous support. Another reason could be the partial functionalization of the surface of the catalysts during the acid leaching with 1 M HCl.

In all the five catalysts, a certain amount of N was also detected. The Fe-N/MPC2 catalyst, which is the only catalyst heat treated twice, had the lower N content. The decrease of N content detected by XPS after the second heat treatment in this types of Me-N-C catalysts was also found in other works [25,26]. This effect could be associated with the release of N-containing gases, which in turn contributes to the increase of the specific surface area and pore volume after the second pyrolysis. Similarly, also the decrease of the O content, associated with the release of O-containing gas molecules, could contribute to the specific surface area increase after the second pyrolysis.

All these considerations are also justified by the slight weight loss (about 10%) detected for the sample pyrolyzed twice by TGA (see Fig. 1c).

For the catalysts heat treated once, the N at.% content varies from a minimum of 1.8% for Fe-N/MPC1 to a maximum of 3.3% for Fe-N/AB. Therefore, the overall N content is not related to the ORR electroactivity of the catalysts, as also reported in the literature [24–26]. However, considering that in Fe-N/C catalysts the ORR activity is believed to be linked with FeN_4 and/or FeN_{2+2} ensembles embedded the carbon matrix [33], a catalyst with the 100% of the total iron available as active ensembles would have a theoretical Fe/N atomic ratio equal to 0.25. Looking at the ratio between the atomic Fe and N content detected by XPS (see Table 2), our most active catalysts (Fe-N/MPC1 and Fe-N/MPC2, see Section 3.2) are the ones showing a value closer to the theoretical one. However, since electrocatalysis is a superficial phenomenon, this conclusion can be only made if the Fe and N amount detected by XPS are assumed as the real quantities present on the catalyst surface. Being XPS a surface sensitive technique (the depth of the analysis is of about 5–6 nm) [47], this assumption can be considered as a good approximation. In fact, the remaining Fe possibly present but not detected by XPS (i.e., in the form of nanoparticles encapsulated more in depth inside the carbonaceous matrix of the catalyst) [57], will most likely not get in contact with the O_2 diffusing from the bulk of the solution (in case of RDE tests) or from the fuel cell cathode flow channels (in case of PEMFC tests) toward the catalyst surface.

The high-resolution N 1s peaks were analyzed by peak deconvolution, as shown in Fig. 2a–e. The four different components identified were pyridinic-N (N1) pyrrolic-N (N2), graphitic-N (N3) and oxidized-N (N4) [58–60]. Table 3 shows the relative and total (referred to the overall nitrogen content of the sample, see Table 2) amounts of the different nitrogen bond types, with their respective binding energy.

In particular, the pyridinic-N type is the most abundant in all of the catalysts, ranging from 42 to 51 at.%. This could be related to the Phen precursor molecule, in which the N atoms are of pyridinic type. The pyrrolic-N is detected in percentages between 32 and 39%, and the graphitic-N in lower amounts (10–17%). In catalysts Fe-N/CNS and Fe-N/MPC1, a certain amount of oxidized-type N is also detected. This result is in accordance with the fact that these two catalysts were also the ones with the higher amounts of O detected. Thus, part of the O in these catalysts should be bounded directly with N.

Trying to relate the relative and total% of the different N-types with the ORR activity of the catalysts, it is not possible to find out any direct relation. However, in many studies, the electrocatalytic activity towards ORR was attributed to pyridinic-N and pyrrolic-N [25,30,37,61]. Despite the real structure of the ORR active ensem-

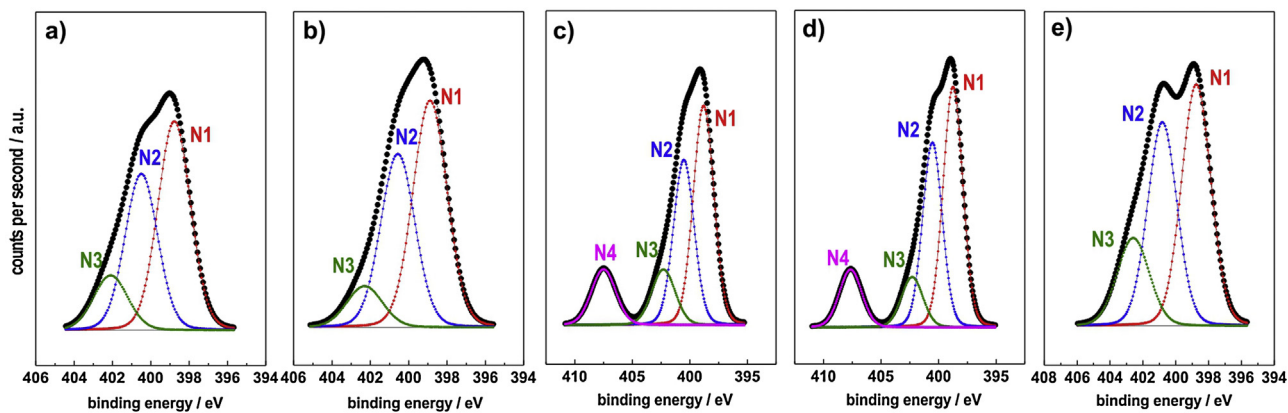


Fig. 2. High resolution N 1s XPS spectra of the catalysts (a) Fe-N/AB; (b) Fe-N/MWCNT; (c) Fe-N/CNS; (d) Fe-N/MPC1; (e) Fe-N/MPC2. The black line is the overall N 1s peak. Red, blue, green and magenta lines correspond to the peak deconvolution into pyridinic-N (N1), pyrrolic-N (N2), graphitic-N (N3) and oxidized-N (N4) components, respectively. (For interpretation of the references to colour in this figure legend, the reader is referred to the web version of this article.)

Table 3

Relative and total contents of the different N types with their respective peak binding energies resulting from the deconvolution of the high-resolution N 1s peak from XPS analysis (N1: pyridinic-N; N2: pyrrolic-N; N3: graphitic-N; N4: oxidized-N).

Catalyst	Binding energy [eV]		Relative content [atomic%]		Total content [atomic%]
	N1	N2	N3	N4	
Fe-N/AB	398.8	400.5	402.1	-	-
	49	37	14	-	
Fe-N/MWCNT	1.62	1.22	0.46	-	-
	398.9	400.6	402.3	-	
Fe-N/CNS	51	39	10	-	407.5
	1.07	0.82	0.21	-	
Fe-N/MPC1	398.8	400.5	402.3	-	407.7
	42	32	12	14	
Fe-N/MPC2	1.18	0.90	0.34	0.39	407.7
	398.8	400.5	402.3	-	
	44	34	10	12	0.22
	0.79	0.61	0.18	-	
Fe-N/MPC2	398.7	400.7	402.5	-	-
	45	38	17	-	
	0.68	0.57	0.25	-	

bles is still not clear and under debate [62], many authors agree with the conclusions that the N atoms which form part of the active ensembles, are of pyridinic type, and are located in the micropores [55]. Therefore, this fact explains the lack of existence of any direct correlation between the total or relative amount of the different N-types and the ORR activity of our catalysts. On the contrary, for these Fe-N/C catalysts, the ORR electroactivity (see Section 3.2), as well as the performance in both DMFC and DEFC (see Section 3.3) is related to the structural features of the carbonaceous supports materials, like the specific surface area and the pore size distribution, and to the weight loss during the pyrolysis.

The Raman spectra were recorded to investigate the phase composition of the C-supports and the Fe-N/C catalysts. In the Raman spectra in Fig. 3, only two peaks are clearly visible. The first one is the graphitic peak (G peak), which lies in the range 1574–1590 cm⁻¹, and corresponds to the in-plane vibration of C atoms in graphene layers. The second one is the “disorder” peak (D peak), which lies in the range 1334–1345 cm⁻¹, and corresponds to a vibration of C atoms at the edges of finite graphene layers, which is detectable only when the graphitic clusters are smaller than about 20 nm [63]. However, to perform a good fitting, two additional peaks were used. The peak in the range 1463–1511 cm⁻¹ (A peak) is attributed to amorphous carbon domains (poorly organized crystallites), while the peak in the range 1175–1204 cm⁻¹ is attributed to C with sp³ bonds or sp² short molecule fragments (rings and/or chains) [64,65]. From the peak position, height and width (full width at half maximum, FWHM), some useful parame-

ters were calculated and listed in Table 4. The position of the D peak is almost the same for all of the samples, while some differences can be noticed for the G peak. In particular, the commercial supports (AB and MWCNT) have the D peak at lower Raman shifts compared to the home-made carbon materials prepared by silica templating method. As explained by Ferrari and Robertson [66], an increase in the G peak position occurs when moving from more ordered graphitic domains to smaller nano-crystalline graphitic domains, thus suggesting that in CNS and MPC contain a higher amount of low-size graphitic domains than MWCNT and AB. This effect could be due to the dependence of the growth of the carbon replica on the silica template morphology [65].

The ratio of the intensity of the D and G peaks (I_D/I_G) is usually assumed in the literature as a parameter related to the disorder degree of the crystalline structure of a carbonaceous material [41]. The disorder of the graphene sheets could be ascribed to the high amount of edges (due to the smaller size of the graphitic domains) and to the presence of heteroatoms [65].

However, all of our catalysts exhibit similar I_D/I_G values close to 1, except MWCNT and Fe-N/MWCNT, which have a higher value close to 1.2, attributable to the enrolled structure of the graphitic planes in MWCNT. Another parameter attributable to the disorder of the carbon structure is the ratio of the FWHM of the D and G peaks (w_D/w_G). In this case, the difference between the catalysts is more evident (see Table 4). In fact, the width of the D peak for both CNS and MPC supports (and their respective Fe-N/C catalysts) is higher than for AB and MWCNT (see also Fig. 3). On the contrary,

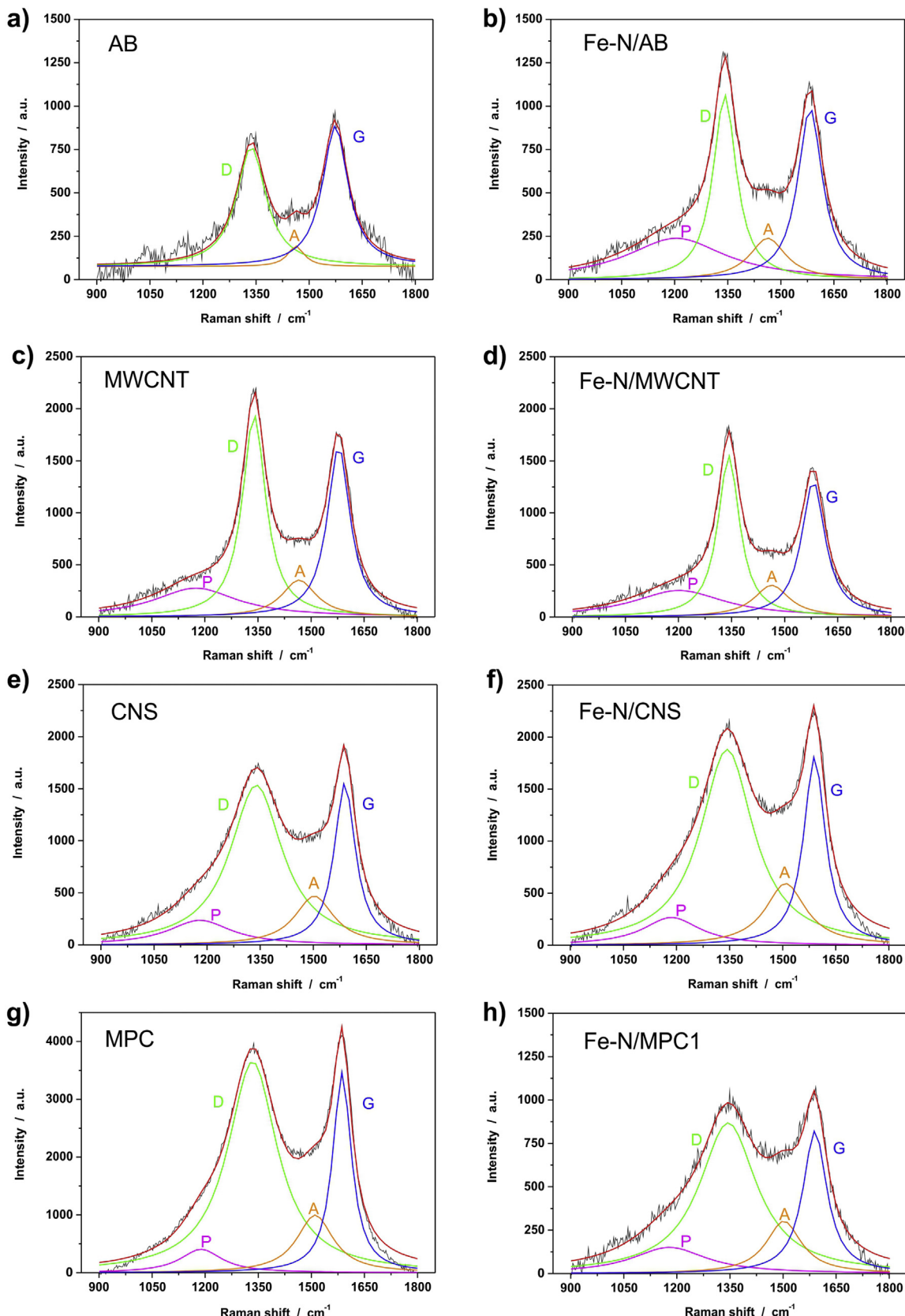


Fig. 3. Fitting of the Raman spectra peaks between 900 and 1800 cm^{-1} for the four different carbon supports and their respective Fe-N/C catalysts (pyrolyzed once). The red line represents the overall fitted peak. Green, blue, orange and magenta lines correspond to the deconvolution into the disorder (D), graphitic (G), amorphous (A) and sp^3 (P) peaks, respectively. (For interpretation of the references to colour in this figure legend, the reader is referred to the web version of this article.)

Table 4

Parameters calculated from the fitting of the Raman spectra and weight loss% from TGA for the C-supports and the Fe-N/C catalysts.

Catalyst	D peak [cm ⁻¹]	G peak [cm ⁻¹]	I_D/I_G	w_D/w_G	I_A/I_G	weight loss [%]
AB	1337	1574	0.90	1.15	0.21	–
MWCNT	1339	1578	1.23	1.00	0.22	–
CNS	1339	1589	1.00	2.48	0.30	–
MPC	1334	1587	1.05	2.65	0.28	–
Fe-N/AB	1342	1583	1.07	0.94	0.24	38.9
Fe-N/MWCNT	1342	1581	1.20	0.92	0.23	37.4
Fe-N/CNS	1343	1591	1.00	2.46	0.32	43.8
Fe-N/MPC1	1345	1590	1.06	2.40	0.36	47.3

the widths of the G peaks of the different samples is more similar to each other. In a previous work [63], a higher w_D/w_G ratio in the C-support was found to be related to both a higher weight loss during the pyrolysis in the catalyst synthesis and to a higher ORR activity.

The ratio of the intensity of the A and G peaks (I_A/I_G) is another parameter that can be associated to the disorder degree of a carbonaceous structure. As evident in Fig. 3, and summarized in Table 4, this ratio is higher for CNS and MPC and also for their respective Fe-N/C catalysts, while MWCNT and AB (and their respective catalysts) show lower I_A/I_G values.

The results in Fig. 1c, showing the TGA of the precursors of the five different catalysts, indicate that the weight loss trend for the precursors of the catalysts pyrolyzed once (Fe(III)-Phen complex + C-support) can be divided in 3 main steps. The first one at 100 °C corresponds to the evaporation of the adsorbed moisture. The second step occurs in the temperature range 200–400 °C, and could be attributed to the partial sublimation of the Phen precursor [24,25]. Interestingly, using the MWCNT and AB supports, the weight loss in this temperature range is higher than for CNS and MPC. This could be ascribed to the lower surface area and the lower content of small-sized pores of the first two supports, which can consequently “store” in depth in their porous structure a lower amount of Fe-Phen precursor. As a consequence, the Phen could be more prone to sublimate at lower temperatures. The third weight loss step occurs above 400 °C, and could be attributed to the degradation of Phen and the following formation of cracking products due to the reducing conditions, associated with the carbonization and the incorporation of N and Fe functionalities on the C-support surface. This process is most likely associated with the formation of the ORR active ensembles. In fact, as known from the literature, the most active Fe-N/C catalysts are obtained after pyrolysis at temperatures higher than 600 °C where the carbonization preferentially occurs [39]. The weight loss in this third step is higher for CNS- and MPC-derived catalysts. This could be a consequence of the lower weight loss at lower temperatures for these samples, which thus have still a higher Fe-Phen complex available for the formation of active ensembles.

Fe-N/MPC1 was pyrolyzed after the acid washing to obtain Fe-N/MPC2, and the results of the TGA simulating this pyrolysis are also shown in Fig. 1c. It is evident that the shape of this TGA curve is completely different from the ones of the precursors pyrolyzed to obtain the other catalysts, since no more Fe-Phen complex was present. In this case, only a slight weight loss of about 10% is observed, mainly attributable to the decomposition of some part of the carbonaceous matrix of Fe-N/MPC1, associated to the release of O- and N-containing gases, which confirms both the higher surface area and the lower O and N content of Fe-N/MPC2 compared to Fe-N/MPC1 (see Tables 1 and 2).

As evident from the results of the TGA (see Fig. 1c and Table 4), there is a relation between the weight loss during the pyrolysis and the ORR activity of the Fe-N/C catalysts (see Table 5). Jaouen and Dodelet found a similar correlation for a wide variety of carbonaceous materials [63].

From the results of the Raman analysis and TGA, we can conclude that the w_D/w_G ratio (considered as a measure of the disorder of the carbonaceous material) of both the C-supports and the Fe-N/C catalysts, as well as the weight loss during the pyrolysis are somehow related to the ORR activity of the final catalysts. In particular, the higher the disorder in the C-support and Fe-N/C catalyst, the higher the weight loss, and, at the same time, the higher the ORR activity of the catalyst. These effects indicate that the presence of a high disordered phase in the C-support leads to the formation of a higher number of ORR active ensembles. In turn, this fact is associated with a higher weight loss, which is a consequence of the partial decomposition of both the C-support and the Fe-Phen complex during the pyrolysis. Thus, a higher weight loss could be linked with a higher reactivity of the disordered C (compared to the more ordered “graphitic” C) with the Fe-Phen and with the gas products evolved during the pyrolysis [63].

3.2. RDE test

The ORR activity of the Fe-N/C catalysts was tested in acidic and alkaline medium by a RDE equipment. Fig. 4a and b shows the results of the staircase voltammetry (SV), in comparison with a commercial Pt/C catalyst. Table 5 summarizes the ORR performance of the different Fe-N/C catalysts in terms of onset potential (E_{on}) and half-wave potential ($E_{1/2}$). E_{on} is defined as the potential required to generate a current density of 0.1 mA cm⁻² in a steady-state RDE experiment [67] and $E_{1/2}$ is the potential required to get half the maximum current density in the polarization curve. For all of the catalysts the ORR process is diffusion-controlled at high overpotentials (Fig. 4a and b). At intermediate overpotentials, the current density is under a mixed diffusion-kinetic control. In alkaline conditions, due to the lower ORR overpotential, the diffusion limited current density region is more evident, and all of the Fe-N/C catalysts have a well-developed current density plateau. On the other hand, in acidic conditions, this plateau is less extended, suggesting that the current density is under mixed diffusion-kinetic control over a wider range of potential, especially for the less active catalysts. This is a consequence of the sluggish ORR kinetics in acidic medium.

In acidic medium, the activities of the catalysts pyrolyzed once are considerably different from one another (Fig. 4a and c). Among those catalysts, the most active is Fe-N/MPC1, which has 100 mV higher E_{on} and 190 mV higher $E_{1/2}$ in comparison with the less active catalyst, that is Fe-N/AB. Considering that all of the catalysts were synthesized in the same way, it is evident how the C-support plays a crucial role in the ORR electroactivity. The use of a C-support with a high specific surface area and an ordered porous structure seems to be useful to allow the formation of a higher number of active ensembles and to favor their accessibility to the reactants.

The exposure of the catalyst to a second pyrolysis during the synthesis (Fe-N/MPC2) results in a gain of 10 mV in E_{on} and of 20 mV in $E_{1/2}$ compared to Fe-N/MPC1. This slight increase of the performance can be ascribed to the increase of the spe-

Table 5

Onset potentials (E_{on}), half-wave potentials ($E_{1/2}$) and Tafel slopes in the low (LO) and high (HO) overpotential regions of the different Fe-N/C catalysts calculated from the data measured in RDE in acid and alkaline conditions.

Acidic medium (0.5 M H ₂ SO ₄)				
Sample	E_{on} [V vs RHE]	$E_{1/2}$ [V vs RHE]	Tafel slope – LO [mV dec ⁻¹]	Tafel slope – HO [mV dec ⁻¹]
Fe-N/AB	0.71	0.49	133	195
Fe-N/MWCNT	0.74	0.53	119	218
Fe-N/CNS	0.77	0.60	102	174
Fe-N/MPC1	0.81	0.68	78	174
Fe-N/MPC2	0.82	0.70	76	155
Pt cathodic scan	0.87	0.76	60	202
Pt anodic scan	0.93	0.82	63	126

Alkaline medium (0.1 M KOH)				
Sample	E_{on} [V vs RHE]	$E_{1/2}$ [V vs RHE]	Tafel slope – LO [mV dec ⁻¹]	Tafel slope – HO [mV dec ⁻¹]
Fe-N/AB	0.92	0.81	75	83
Fe-N/MWCNT	0.97	0.84	70	136
Fe-N/CNS	0.96	0.85	62	141
Fe-N/MPC1	0.98	0.86	71	164
Fe-N/MPC2	1.00	0.88	73	145
Pt cathodic scan	1.00	0.89	67	116
Pt anodic scan	1.01	0.92	58	128

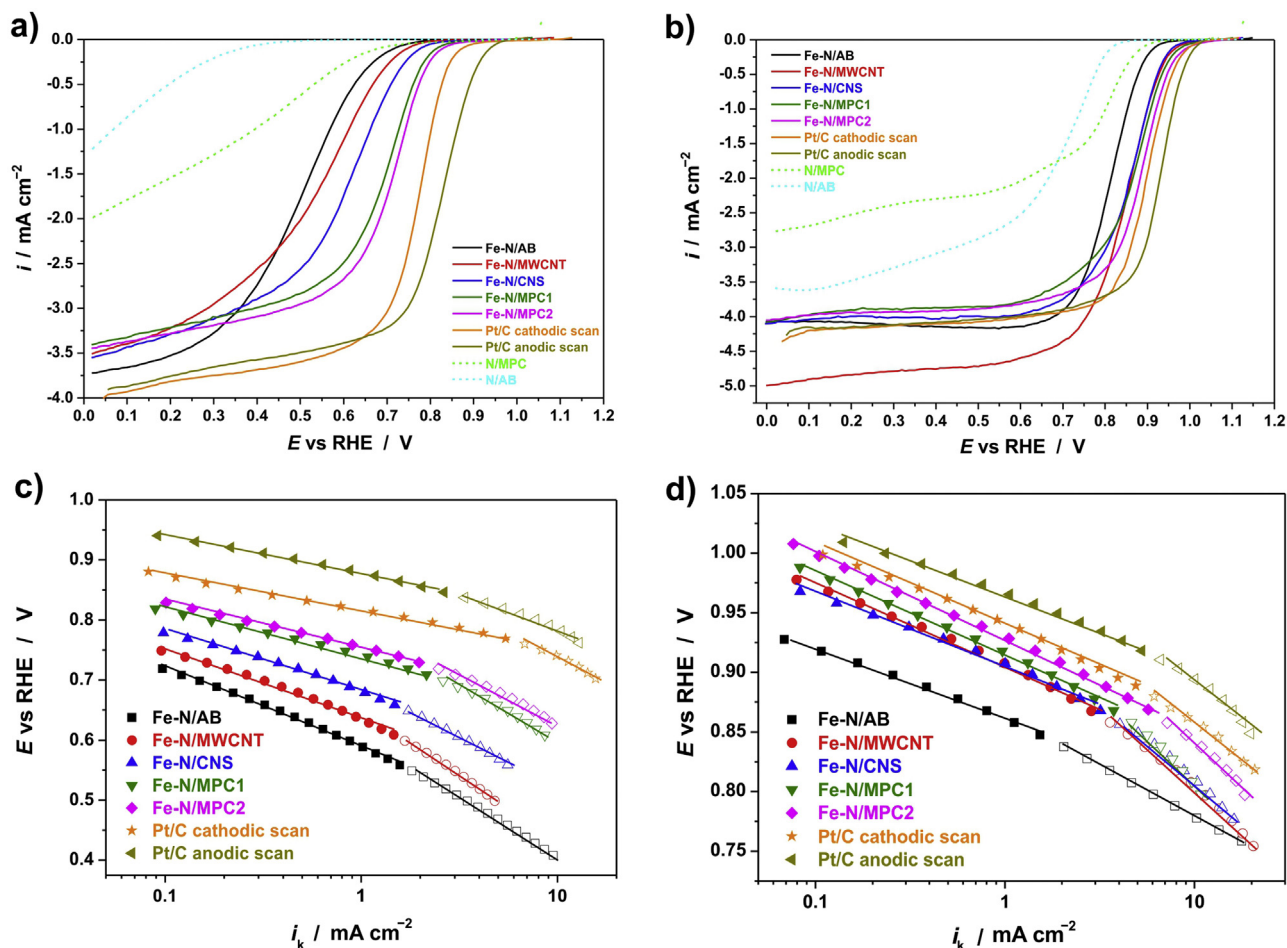


Fig. 4. Steady state polarization curves (10 mV potential step, 10 s holding time) for the five Fe-N/C catalysts, the two N/C catalysts, and a commercial 20 wt.% Pt/C catalyst (in both potential scan directions) recorded in RDE at 900 rpm in O₂-saturated (a) 0.5 M H₂SO₄ and (b) 0.1 M KOH. Tafel plots of the Fe-N/C and Pt/C catalysts derived from the steady state polarization curves after mass-transport contribution correction in (c) acid and (d) alkaline conditions.

cific surface area and porosity and of the Fe/N atomic ratio (Table 2), which could correspond to an increase of the active sites.

The catalysts have a much higher ORR activity in alkaline than in acidic conditions, as typically observed for this type of Fe-N-doped carbonaceous materials [24,68,69]. In particular, the E_{on} are

almost 200 mV higher in alkaline than in acidic medium. In alkaline conditions, the differences among the ORR electroactivity of the five Fe-N/C catalysts are less evident. Fe-N-/MWCNT, Fe-N/CNS, and Fe-N/MPC1 have practically the same activity, being their E_{on} and $E_{1/2}$ only 10 mV different from each other. Fe-N/MWCNT catalyst has a higher diffusion-limited current density, which could be caused by the bad dispersion of the MWCNT-based catalyst in the ink, and consequently also onto the glassy carbon surface of the RDE. In fact, MWCNT tend to form agglomerates which are very difficult to disperse in the ink solution. The presence of these agglomerates, that are also visible during the preparation of the electrode, does not allow to have a thin, homogeneous, and smooth surface of the RDE electrode after the deposition of the catalyst on it. This fact can locally enhance the turbulence in proximity of the RDE surface during rotation, locally increasing the mass transport of the O_2 and resulting in a higher limiting current value, as demonstrated in the literature [70].

As found for the test in acidic medium, Fe-N/AB catalyst has the lowest ORR activity also in alkaline conditions. The effect of the second pyrolysis on the ORR activity is evident also in alkaline, providing a slight increase of 20 mV in both the E_{on} and $E_{1/2}$, as obtained in acidic condition.

Observing the results of the SV recorded for the two samples prepared without Fe (N/AB and N/MPC), it is even more evident as the influence of the C-support on the ORR activity is remarkable. The difference between the two selected C-supports is much wider in acid than in alkaline medium, due to the intrinsic electroactivity towards ORR of N-doped C-based materials in alkaline medium. This fact helps to better explain and understand the differences in the measured ORR activities in RDE as well as the performances in direct alcohol fuel cells in the two different media. The ORR activity performance of the catalysts prepared using Fe is considerably higher compared to the catalysts prepared without Fe in both media. However, the improvement is much more evident in acidic than in alkaline conditions, confirming that the choice of a proper carbonaceous support plays a considerably more important role in acidic environment.

One reason for the less evident differences among the activities of the Fe-N/C catalysts in alkaline conditions could be the intrinsic ORR catalytic activity of the N-doped carbonaceous materials, which promote the $2 e^-$ reduction of O_2 to HO_2^- in alkaline medium [71]. As described in the literature, other reasons for the enhanced activity of Fe-N/C catalysts in alkaline conditions could be the occurrence of the ORR by the “outer-sphere” mechanism. In fact, this mechanism is promoted by the presence of the carbon support in alkaline conditions (*i.e.*, by the mediation of the quinone/hydroquinone surface functional groups), and the better stabilization of the HO_2^- ion on the Fe-N_x active ensembles [24,68,72]. These effects can “mitigate” the differences between the activities of the different catalysts, which conversely are more evident in acid medium.

As evident from Fig. 4b and d, the performance of the best catalysts (Fe-N/MPC1 and Fe-N/MPC2) in alkaline conditions are almost equal to that of a Pt/C commercial catalyst, making their use as cathodic catalyst in an alkaline PEMFC very promising (see Section 3.3.2).

Observing the Tafel plots in both acid and alkaline medium (Fig. 4c and d, respectively), for all of the catalysts we can identify two different slope regions. At low overpotentials (LO), a first zone is characterized by lower Tafel slope values, while at high overpotentials (HO) the Tafel slope increases. This behavior is analogous to the Pt-based catalysts, where the Tafel slope in the LO region is usually of about 60 mV dec^{-1} , and it almost doubles (about 120 mV dec^{-1}) at higher overpotentials in both acidic and alkaline media [73]. This Tafel slope change for Pt is explained with the

change in the O_2 adsorption from Temkin to Langmuir mechanism with the increase of the overpotential [74,75].

When estimating the ORR activity for Pt-based catalysts, usually the anodic scan direction is analyzed as, in this case, the activity is not affected by oxide layer which is slowly removed when the potential is decreasing. Analyzing both anodic and cathodic sweep directions, the catalysts have a certain hysteresis, which is commonly ascribed to slow removal of surface oxides (hindering the ORR during the negative going sweep) [76]. In this work, we reported the data of the Pt/C catalyst used as comparison in both the potential scan directions. In fact, even if the anodic scan is most favorable for electroactivity, the cathodic scan is more interesting in relation to the operating conditions of a fuel cell cathode.

Regarding the Tafel slopes in alkaline conditions, the values calculated for our Fe-N/C catalysts are similar to that of Pt/C catalyst, except for Fe-N/AB, for which the difference from LO to HO region is not so evident. The activity of this catalyst in alkaline medium was considerably lower compared to Pt, and this could explain its different behavior.

In the case of acidic conditions, the situation is more complicated. In fact, in spite of showing an almost double Tafel slope at HO than at LO, the values in the LO zone are similar to Pt only for the most active catalysts (Fe-N/MPC1 and Fe-N/MPC2, see Table 5). For the other catalysts, these values are higher, being closer to 120 mV dec^{-1} , which is the value of the Pt catalysts in the HO zone. This fact could be explained by the considerably higher E_{on} of these catalysts compared to Pt/C. As a consequence, when the ORR starts to occur on these catalysts, the surface conditions are already more similar to the HO zone for the most active catalysts, and thus the LO region with lower Tafel slopes of about 60 mV dec^{-1} cannot be observed.

3.3. Fuel cell tests

The performances of the Fe-N/C catalysts were evaluated in two different types of fuel cells to better highlight the differences among the different C-supports on the characteristics of the catalyst from a more applicative point of view.

The first type of fuel cell considered was a DMFC operating in acidic conditions (Nafion® 117 membrane). Then, a second series of tests was conducted in a DEFC equipped with an alkaline membrane (PBI doped with KOH) conducting OH^- ions. Since one of the major limitations of DAFC performance is the low kinetic of the alcohol oxidation reaction in acidic media, one can take advantage operating in alkaline media by the faster alcohol oxidation reaction [5], and by the faster ORR kinetic as well.

3.3.1. Acidic DMFC

Fig. 5a shows the results of the DMFC tests with the different Fe-N/C catalysts in terms of polarization and power density curves, together with the results obtained with a commercial 40 wt.% Pt/C catalyst at the cathode as a comparison. Table 6 summarizes the main performance parameters.

The Pt/C catalyst got the best results in terms of power density, while Fe-N/MPC1 was the most performing within our catalysts. Interestingly, the open circuit potential (E_{oc}) values of our Fe-N/C catalysts were almost the same observed for the Pt/C catalyst. However, in RDE, the E_{on} for ORR of Pt/C catalyst was considerably higher than for our non-noble catalysts (see Table 5). This is due to the detrimental effects of methanol crossover, causing a mixed potential at the cathode of the DMFC, and a consequent important performance decrease for Pt [10]. The DMFC prepared using the Fe-N/MPC1 has a maximum power density about 73% than that of Pt/C. Fe-N/MPC2 shows a slightly lower performance, with about 57% maximum power density compared to Pt/C. This result is in disagreement with the results of RDE tests, where the E_{on} and $E_{1/2}$ of

Table 6

Performance parameters for acid DMFC tests in Fig. 5a and alkaline DEFC test in Fig. 5b for the different Fe-N/C catalysts and the commercial Pt/C catalyst.

FC type	Cathode catalyst	E_{oc} [V]	i_{max} [mA cm^{-2}]	P_{max} [mW cm^{-2}]	Specific P_{max} [$\text{W g}_{\text{Pt}}^{-1}$]
Acidic DMFC	Fe-N/AB	0.54	22	2.0	2.0
	Fe-N/MWCNT	0.57	123	7.7	7.7
	Fe-N/CNS	0.60	114	7.6	7.6
	Fe-N/MPC1	0.64	225	22.6	22.6
	Fe-N/MPC2	0.63	222	17.5	17.5
	Pt/C	0.62	274	30.9	15.5
Alkaline DEFC	Fe-N/AB	0.79	152	48.3	36.3
	Fe-N/MWCNT	0.85	230	71.1	53.4
	Fe-N/CNS	0.70	189	48.0	36.1
	Fe-N/MPC1	0.89	258	71.3	53.6
	Fe-N/MPC2	0.87	216	72.8	54.7
	Pt/C	0.86	342	88.9	38.2

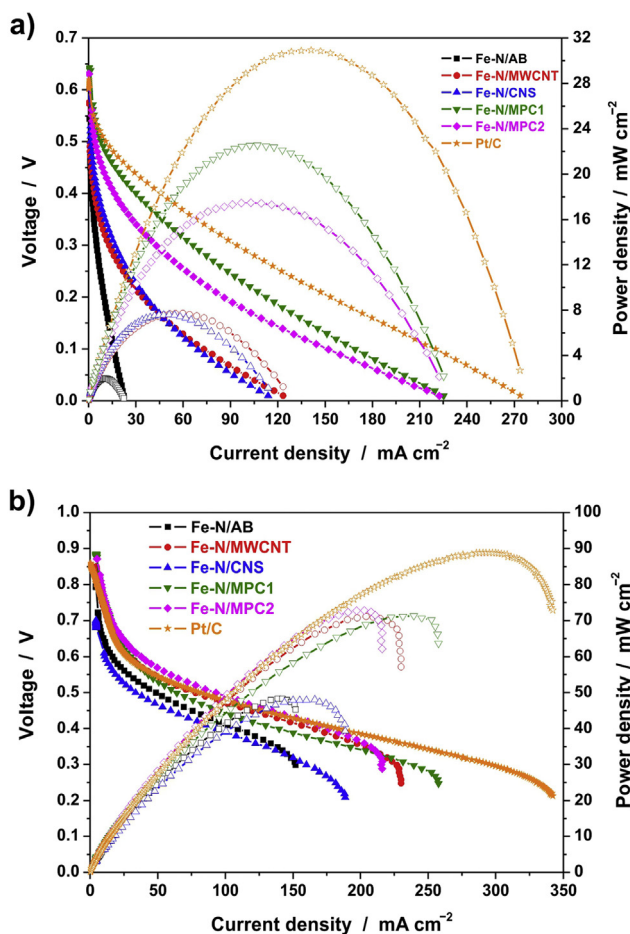


Fig. 5. Polarization curves (open symbols) and power density curves (filled symbols) obtained at 90 °C using the different Fe-N/C catalysts and a commercial Pt/C catalyst at the cathode of (a) acidic DMFC and (b) alkaline DEFC.

Fe-N/MPC2 were slightly better. This fact could be explained by the higher microporosity of Fe-N/MPC2. In fact, in spite of being useful to increase the ORR activity in this type of Me-N-C catalysts, the micropores could be problematic in the fuel cell operation because they are subjected to water flooding. In fact, the water produced at the cathode condenses into micropores, flooding them, with consequent problems of mass transport and performance decay [77]. This opposite behavior in RDE and in PEMFC can also be found in the literature [58], suggesting that better ORR performance in RDE do not automatically mean a better performance in PEMFC. These results

confirm the importance of showing single cell tests in the study of ORR catalysts for PEMFC application.

Fe-N/CNS, Fe-N/MWCNT, and Fe-N/AB catalysts have considerably lower performance, confirming the results of RDE test. The results of Fe-N/AB are particularly bad, probably because of low specific surface area and low micropores content, which result in a formation of a too low number of active ensembles. Considering Fe-N/CNS, its performance is almost similar to that of Fe-N/MWCNT, even if in the RDE test in acidic conditions the former was more active (see Fig. 4a and c). This better performance of Fe-N/MWCNT in single cell test could be ascribed to its better mass transport properties due to higher macropores content (favoring active sites accessibility). A worse intrinsic dispersibility of the material in the ink preparation could be partially the cause of that the DMFC performance of Fe-N/CNS was lower than what expected.

All these considerations point out how different aspects of a Fe-N/C catalyst for ORR have to be taken into account to consider it as a good candidate for application in PEMFC.

Generally speaking, the overall performance of our Fe-N/C catalysts in DMFC was lower compared to Pt/C. Nevertheless, if we normalize the maximum power density to the total Pt amount used to fabricate the MEA (see Specific P_{max} in Table 6) [11] using the two most active catalysts (Fe-N/MPC1 and Fe-N/MPC2), we obtain better performance than with the Pt/C catalyst.

The results described previously are referred to the beginning of the test, and they do not consider the durability, which is a major issue for Pt/C catalysts used at the cathode of DMFC. Thus, a short-term durability test in DMFC developed in our laboratory [10] was carried out for the two most performing catalysts (Fe-N/MPC1 and Fe-N/MPC2), and for the commercial Pt/C catalyst. The rationale behind the design of this durability test is described in our previous work [10]. Fig. 6a–c show the polarization and power density curves of Fe-N/MPC1, Fe-N/MPC2, and Pt/C recorded at the beginning of the test ($t = 0$) with a methanol solution flow rate at the anode of 1 and 5 mL min^{-1} , respectively. Fig. 6a and b also show the polarization curves recorded at regular intervals of 1 h until the end of the test ($t = 3$ h), with a flow rate of 5 mL min^{-1} .

The use of a higher flow rate, should lead to an increase of the kinetics due to a higher flux of reactants to the anodic compartment [78]. However, at the same time, the water and methanol diffusion through the membrane increase significantly, enhancing detrimental effects of the methanol crossover.

The performance of the NNM-based DMFC was only slightly affected by the increase in the methanol solution flow rate at the beginning of the test. In fact, the E_{oc} was practically the same as with the lower flow rate for both Fe-N/MPC1 and Fe-N/MPC2 catalysts, and the maximum power density only decreased from 22.5 to 20.2 mW cm^{-2} for Fe-N/MPC1, and from 17.5 to 15.2 mW cm^{-2} for Fe-N/MPC2, respectively (see Fig. 6d). After 3 h test, the DMFC

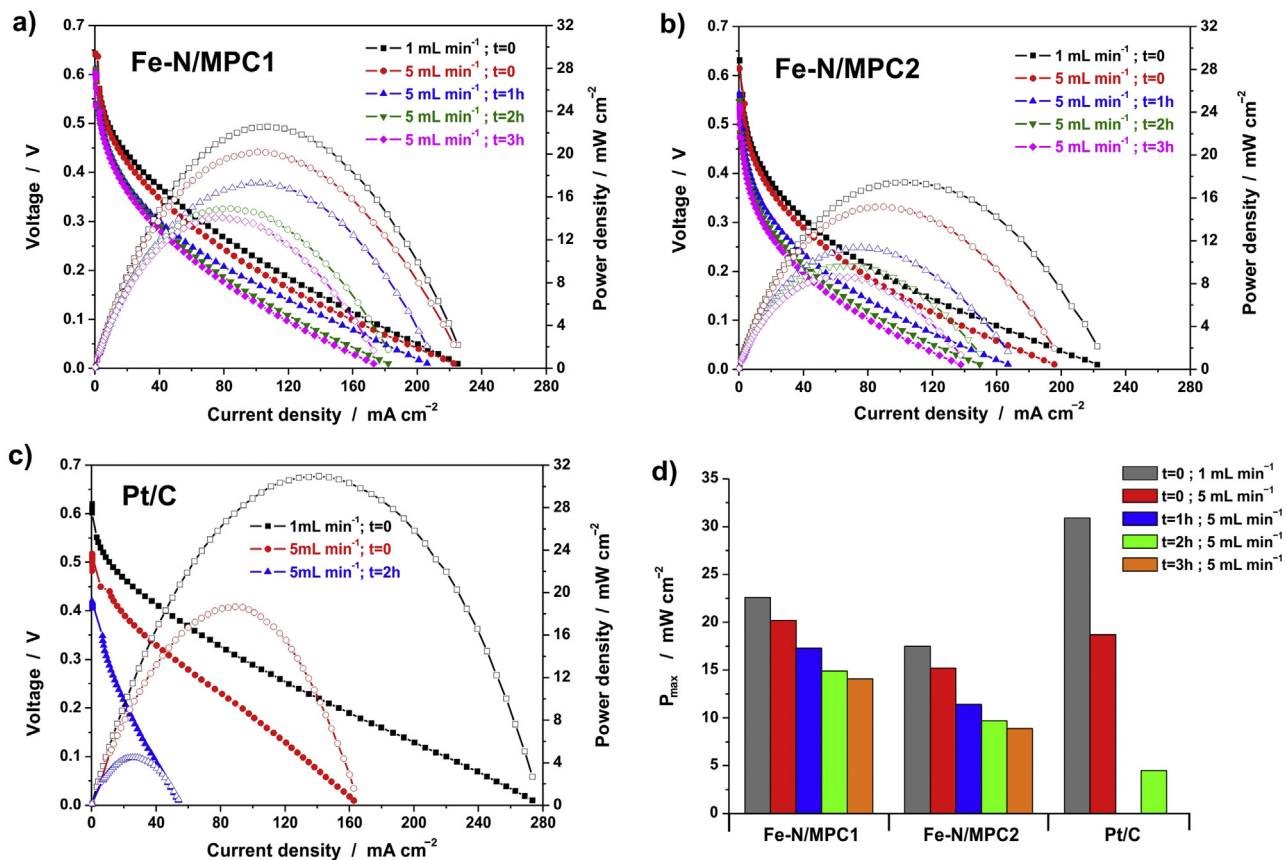


Fig. 6. Short-term durability test in acidic DMFC at 90 °C. Polarization curves (filled symbols) and power density curves (open symbols) for (a) Fe-N/MPC1; (b) Fe-N/MPC2; (c) commercial Pt/C used as cathodic catalysts. (d) Maximum power density decays during DMFC short-term durability tests.

maximum power density was 14.1 mW cm⁻² for Fe-N/MPC1 and 8.6 mW cm⁻² for Fe-N/MPC2, respectively.

Conversely, the performance of the Pt/C-based DMFC remarkably decreased after the 5-fold increasing of the methanol flow rate at $t=0$. In fact, the E_{oc} decreased by 90 mV (from 0.61 to 0.52 V) and the maximum power density dropped down from 30.9 to 18.7 mW cm⁻². Thus, for Pt/C, the negative effect of the increase of the methanol flow rate at the anode was much more evident than for our NNM catalysts. Moreover, after only 2 h test, the maximum power density decreased to 4.5 mW cm⁻² and the E_{oc} further decreased of 100 mV compared to the beginning of the test (see Fig. 6d).

The short-term durability results obtained with the two Fe-N/MPC catalysts are considerably better compared to that of Pt/C, pointing out once more the advantage of using well-tuned NNM catalysts at the cathode of DMFC. In addition to their low cost compared to Pt and their higher availability, these Fe-N/C catalysts have a considerably higher stability during DMFC operation as a consequence of their high tolerance to methanol crossover [11,79]. The durability test results for both Fe-N/MPC1 and Fe-N/MPC2 were better than for another Fe-N-C catalyst produced by our group [10]. Nevertheless, these Fe-N/C catalysts still need improvements: first, their ORR electroactivity in acidic media compared to Pt is low, as well as the stability of active sites. Second, the structural and morphological features (such as a porous structure) are great issues and need further improvements to avoid mass transport problems during PEMFC operation (i.e., water flooding phenomena, O₂ accessibility to active sites) [77,80,81]. In fact, as discussed in the literature, even if the methanol tolerance has been widely demonstrated [11,79,82,83], various other phenomena are believed to be responsible for the still low durability of these Me-

N-C catalysts in DMFC. In particular, the active sites destruction in acidic media could play an important role in the DMFC performance decrease (e.g., by dissolution or chemical leaching-out of iron active center away from the nitrogen coordination [84,85], protonation of pyridinic-N [86], Fenton-type reaction producing attacking radicals [77,87,88], also causing membrane degradation [89], and carbon corrosion phenomena). Irreversible capillary condensation inside micropores [77,81,90,91], where ORR active sites are mostly located [58,92], could be another cause of this performance decrease.

3.3.2. Alkaline DEFC test

The performance of the Fe-N/C catalysts was also tested in an alkaline DEFC fed with a 2 M methanol – 2 M KOH solution. KOH was added to the ethanol solution to provide an excess of OH⁻ ions in contact with the membrane. This helps to enhance both the membrane conductivity and the reaction kinetics [93].

Fig. 5b shows the polarization and power density curves resulting from this test, together with the results of the same test performed on a DEFC prepared with a Pt/C commercial catalyst at the cathode. In the low-intermediate current density region (until about 200 mA cm⁻²), the performances of the Fe-N/MWCNT, Fe-N/MPC1 and Fe-N/MPC2 catalysts are comparable to that of Pt/C. For these catalysts, the E_{oc} are also comparable with Pt/C. In particular, the performance of Fe-N/MPC2 is even slightly better than Pt/C.

On the contrary, for current densities higher than 200 mA cm⁻², the cell performances rapidly decrease. In fact, immediately after the attainment of the maximum power density, the polarization curves show a steep decrease. This behavior suggests that the cell is highly affected by mass transport problems at high current density

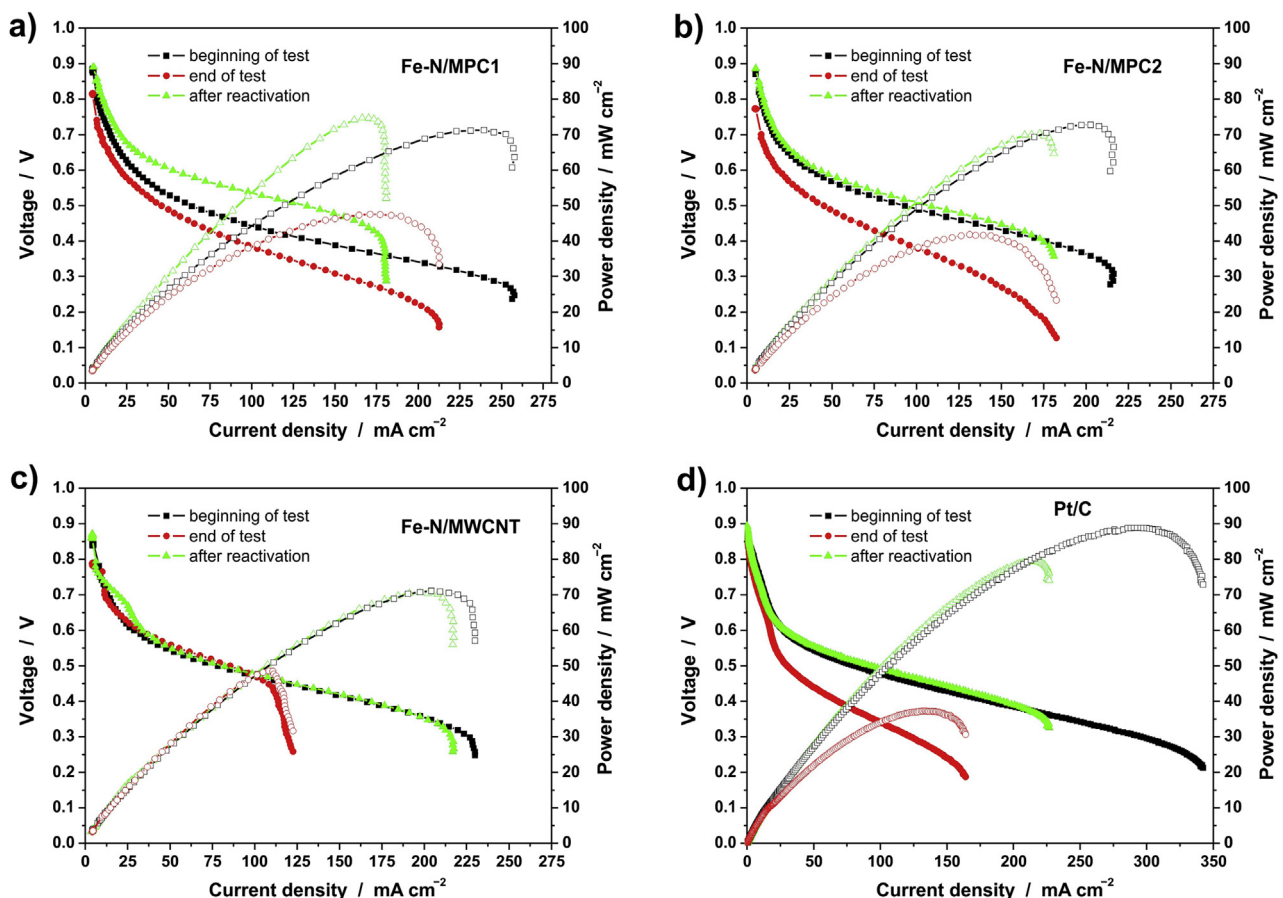


Fig. 7. Short-term durability test in alkaline DEFC at 90 °C. Polarization curves (filled symbols) and power density curves (open symbols) recorded at the beginning of the test (black), at the end of the test (red), and after purge-drying reactivation (green). (a) Fe-N/MPC1; (b) Fe-N/MPC2; (c) Fe-N/MWCNT; (d) commercial Pt/C used as cathodic catalysts. (For interpretation of the references to colour in this figure legend, the reader is referred to the web version of this article.)

values [94]. These mass transport limitations could be ascribed to the diffusion of the oxygen into the cathode catalyst layer, which could be hindered by the high ionomer content [93] and by the microporous structure of the catalyst. Another reason could be the cathode flooding [77,81], which is reported in the literature to be more relevant exactly in the intermediate current density range (around 200 mA cm⁻²) [95], as confirmed by our results. In fact, interestingly, all of our catalysts start to be affected by mass transport problems when the current density approaches 200 mA cm⁻². However, since in alkaline membrane fuel cells water is generated at the anode, the occurring of anode flooding at high current density, as well as problems due to the lack of OH⁻ conducting ionomer in both catalytic layers should not be disregarded [93].

These results in terms of power density (around 72 mW cm⁻²) and polarization curve shape are comparable to the best “State-of-the-Art” results available in the literature for alkaline membrane DEFC using an NNM catalyst at the cathode [73,96].

The performance of Fe-N/CNS and Fe-N/AB catalysts are lower, both showing about 50 mW cm⁻² maximum power density. This result is not surprising for Fe-N/AB, being its performance in RDE in alkaline condition also lower compared to the other catalysts (see Fig. 4b and Table 5). However, its performance is not as bad as it was in the case of DMFC test in acid conditions. Regarding Fe-N/CNS, its performance is lower than what expected, as also found in DMFC test.

Also in this case, as previously found for DMFC test in acidic conditions, referring the maximum power density to the total mass of Pt used for the MEA fabrication, the performance of our best cata-

lysts overcome the one of Pt/C. In fact, for Fe-N/MWCNT, Fe-N/MPC1 and Fe-N/MPC2, the specific maximum power density (referred to the unit mass of Pt in the MEA) is of about 54 W g_{Pt}⁻¹ (considering 1.33 mg_{Pt} cm⁻² at the anode), while for the commercial Pt/C the value is 38.2 W g_{Pt}⁻¹ (considering 1.33 mg_{Pt} cm⁻² at the anode and 1 mg_{Pt} cm⁻² at the cathode).

The performance of these Fe-N/C catalyst in alkaline DEFC, especially at low-intermediate current density, are very promising. However, they could likely be improved by performing an optimization of the electrode preparation in terms of both catalyst loading and ionomer content [10,11]. Moreover, the type of ionomer to be used for the preparation of the catalyst ink instead of Nafion® (i.e., an OH⁻ conducting ionomer) is another parameter that influences the performance of alkaline DEFC. In fact, the ionomer should preferably be of the same type, or at least compatible with the material of the electrolyte membrane [97].

Durability measurements in alkaline DEFC represent a complicated issue to be overcome, especially regarding the possibility to draw conclusions about the durability of the catalysts. For this purpose, in fact, it would be necessary to operate with a very stable anionic membrane (as Nafion® is as protonic conducting membrane), but this is still a great challenge at the present time.

Nowadays, work is underway to obtain anion exchange membranes containing fixed OH⁻ conducting groups (i.e. quaternary ammonium) that could facilitate the movement of OH⁻ ions [98,99]. Unfortunately, at the present time, there is not any material with these properties widely commercialized and available on the market. Therefore, in this work, we used PBI doped with KOH as the

anion exchange membrane, which does not contain fixed OH[−] conducting functional groups in their structure. This type of membranes has stability issues, so durability measurements are a serious problem, and thus it was not possible to carry out a specific durability testing protocol, *i.e.* operating the fuel cell at a constant potential during a certain time, as previously done for acidic DMFC. On the other hand, as previously stated, these Fe-N/C catalysts show additional stability problems, like the flooding due to their high content of small size pores, and the Fe-based active ensembles instability. In spite of these catalysts show very good ORR activity in half cell configuration (RDE), they show instability problems once tested in single-cell configuration. In addition, since the measurements are made under continuous flow of ethanol dissolved in water, this could increase even more these flooding problems.

However, we report in Fig. 7 the alkaline DEFC polarization and power density curves of the catalysts which showed the best performance in DEFC tests (see Fig. 5b), that is Fe-N/MPC1, Fe-N/MPC2, and Fe-N/MWCNT. The results obtained for the same test using the Pt/C catalyst are also shown for comparison. Fig. 7 shows the curves at the beginning of the test, after a few hours of work (20 consecutive recording of polarization curves interspersed by a rest at E_{oc}), and after a purge/drying (flowing dry N₂ at 90 °C for 30 min) and subsequent reactivation.

It is evidenced how, after only few polarization scans, all the DEFCs show important decreases in their performance. Another detail that was experienced in the laboratory was that, after a purge and reactivation, the performance of the DEFC can be recovered again, obtaining polarization and power density curves similar to those obtained at the beginning of the test. These results imply that it is not the catalytic material which causes the performance loss, but rather that it is the system itself that gives rise to these large decays that prevent the possibility of a good measure of durability of this type of devices under continuous operation.

This instability of the alkaline DEFC system could be tentatively attributed to:

- instability of the membrane conductivity performance [100];
- incompatibility (poor affinity) between the material of the membrane (PBI doped with KOH) and the ionomer used to prepare the catalyst ink (Nafion®);
- partial detachment/separation of the electrodes from the membrane due to the absence of hot pressing during the MEA preparation;
- too high rate of formation of water as reaction product at the anode (considering the enhanced kinetics of both EOR and ORR) causing instability.

4. Conclusions

By concluding, the characteristics of the C-support are essential to reach better ORR activity. In particular, the support morphology and structural features like the specific surface area and pore size distribution, as well as the weight loss during the pyrolysis and the w_D/w_C ratio in the C-supports and in the final Fe-N/C catalysts, were found to be important parameters to synthesize more active catalysts.

These points have much more influence in acid than in alkaline conditions. In fact, at low pH, due to the slower kinetics of ORR, the distribution and accessibility of the active sites are more important and limiting factors. This result was confirmed not only by the polarization curves recorded in RDE in 0.5 M H₂SO₄ solution, but also by the acidic electrolyte membrane DMFC tests.

Otherwise, in alkaline conditions, the enhanced ORR kinetics caused by the intrinsic properties of the carbon and N-doped carbon-based materials, makes the influence of the C-support char-

acteristics on the final ORR activity less evident in both RDE and alkaline electrolyte membrane DEFC tests.

In acidic membrane DMFC, if one only cares about the cost reduction, choosing for example a carbon black support (e.g. AB), the risk of producing a catalyst with a too poor final ORR activity is high. Therefore, much attention has to be paid in the choice of an adequate C-support, and in its synthesis. In this regard, the use of a sacrificial template like a mesoporous silica to obtain the final desired structural features was demonstrated to be effective.

Conversely, in alkaline membrane DEFC, since the difference in ORR electroactivity attributable to the C-support is lower, a good choice could be to use a cheaper support, assuring at the same time a good performance (*i.e.*, MWCNT in this work).

These results highlight the great potentialities of the use of Me-N-C non-noble metal catalysts for ORR in DAFC. Moreover, in the case of DMFC the high methanol tolerance, and the consequent higher durability compared to Pt/C catalysts was also evidenced. In alkaline DEFC the durability measurement is problematic. Even if the initial performance suffers a fast decrease, after drying, purging and a new reactivation, almost the same initial performance can be obtained. This behavior suggests that the catalyst is mostly not losing its activity, while the DEFC system is not stable.

Acknowledgments

This work was supported by the Italian Ministry of Education, University and Research [PRIN NAMEDPEM, “Advanced nanocomposite membranes and innovative electrocatalysts for durable polymer electrolyte membrane fuel cells”, grant n. 2010CYTAW]; the Madrid Regional Research Council (CAM) [RESTOENE-2 grant n. S2013/MAE2882]; the Spanish Economy and Competitiveness Ministry [ENE2013 grant n. 42322-R]. Dr. Carlos Palacio from the Universidad Autónoma de Madrid (Spain) is gratefully acknowledged for Raman measurements.

References

- [1] S. Specchia, C. Francia, P. Spinelli, Polymer electrolyte membrane fuel cells, in: J. Zhang, L. Zhang, H. Liu, A. Sun, R.-S. Liu (Eds.), *Electrochem. Technol. Energy Storage Convers.*, WILEY-VCH Verlag, Weinheim, 2011, pp. 601–670, <http://dx.doi.org/10.1002/9783527639496>.
- [2] S.K. Nataraj, C.H. Wang, H.C. Huang, H.Y. Du, S.F. Wang, Y.C. Chen, L.C. Chen, K.H. Chen, Highly proton-selective biopolymer layer-coated ion-exchange membrane for direct methanol fuel cells, *ChemSusChem* 5 (2012) 392–395, <http://dx.doi.org/10.1002/cssc.201100366>.
- [3] A.H.A. Monteverde Videla, L. Osmieri, S. Specchia, Non-noble metal (NNM) catalysts for fuel cells: tuning the activity by a rational step-by-step single variable evolution, in: J.H. Zagal, F. Bedioui (Eds.), *Electrochem. N4 Macrocycl. Met. Complexes – Vol. 1* Energy, Springer, 2016, 2017, pp. 69–102, <http://dx.doi.org/10.1007/978-3-319-31172-2>.
- [4] A. Mahmood, M.A. Scibioh, J. Prabhuram, M.-G. An, H.Y. Ha, A review on durability issues and restoration techniques in long-term operations of direct methanol fuel cells, *J. Power Sources* 297 (2015) 224–241, <http://dx.doi.org/10.1016/j.jpowsour.2015.07.094>.
- [5] E. Antolini, E.R. Gonzalez, Alkaline direct alcohol fuel cells, *J. Power Sources* 195 (2010) 3431–3450, <http://dx.doi.org/10.1016/j.jpowsour.2009.11.145>.
- [6] L. Osmieri, A.H.A. Monteverde Videla, S. Specchia, The use of different types of reduced graphene oxide in the preparation of Fe-N-C electrocatalysts: capacitive behavior and oxygen reduction reaction activity in alkaline medium, *J. Solid State Electrochem.* 20 (2016) 3507–3523, <http://dx.doi.org/10.1007/s10008-016-3332-2>.
- [7] A.L. Mohana Reddy, N. Rajalakshmi, S. Ramaprabhu, Cobalt-polypyrrole-multiwalled carbon nanotube catalysts for hydrogen and alcohol fuel cells, *Carbon N. Y.* 46 (2008) 2–11, <http://dx.doi.org/10.1016/j.carbon.2007.10.021>.
- [8] Non-Noble Metal Fuel Cell Catalysts, in: Z. Chen, J.-P. Dodelet, J. Zhang (Eds.), *WILEY-VCH Verlag, Weinheim*, 2014.
- [9] D. Sebastián, V. Baglio, S. Sun, A.C. Tavares, A.S. Aricò, Graphene-supported stoichiometric sodium tantalate as a methanol-tolerant, non-noble-metal catalyst for the electroreduction of oxygen, *ChemCatChem* 7 (2015) 911–915, <http://dx.doi.org/10.1002/cctc.201403026>.
- [10] L. Osmieri, R. Escudero-cid, A.H.A. Monteverde, P. Ocón, S. Specchia, Performance of a Fe-N-C catalyst for the oxygen reduction reaction in direct methanol fuel cell: cathode formulation optimization and short-term

durability, *Appl. Catal. B Environ.* 201 (2017) 253–265, <http://dx.doi.org/10.1016/j.apcatb.2016.08.043>.

[11] D. Sebastián, V. Baglio, A.S. Aricò, A. Serov, P. Atanassov, Performance analysis of a non-platinum group metal catalyst based on iron-aminoantipyrine for direct methanol fuel cells, *Appl. Catal. B Environ.* 182 (2015) 297–305, <http://dx.doi.org/10.1016/j.apcatb.2015.09.043>.

[12] H. Liu, C. Song, L. Zhang, J. Zhang, H. Wang, D.P. Wilkinson, A review of anode catalysis in the direct methanol fuel cell, *J. Power Sources* 155 (2006) 95–110, <http://dx.doi.org/10.1016/j.jpowsour.2006.01.030>.

[13] A.Y. Tsividze, M.R. Tarasevich, A.V. Kuzov, I.A. Romanova, D.A. Pripadchev, New nanosized cathode electrocatalysts tolerant to ethanol, *Dokl. Phys. Chem.* 421 (2008) 166–169, <http://dx.doi.org/10.1134/S0012501608070038>.

[14] G. Merle, M. Wessling, K. Nijmeijer, Anion exchange membranes for alkaline fuel cells: a review, *J. Membr. Sci.* 377 (2011) 1–35, <http://dx.doi.org/10.1016/j.memsci.2011.04.043>.

[15] J.R. Varcoe, P. Atanassov, D.R. Dekel, A.M. Herring, M.A. Hickner, P.A. Kohl, A.R. Kucernak, W.E. Mustain, K. Nijmeijer, K. Scott, T. Xu, L. Zhuang, Anion-exchange membranes in electrochemical energy systems, *Energy Environ. Sci.* 7 (2014) 3135–3191, <http://dx.doi.org/10.1039/C4EE01303D>.

[16] A.V. Tripkovic, K.D. Popovic, B.N. Grgur, B. Blizanac, P.N. Ross, N.M. Markovic, Methanol electrooxidation on supported Pt and PtRu catalysts in acid and alkaline solutions, *Electrochim. Acta* 47 (2002) 3707–3714, [http://dx.doi.org/10.1016/S0013-4686\(02\)00340-7](http://dx.doi.org/10.1016/S0013-4686(02)00340-7).

[17] Q. Li, R. Cao, J. Cho, G. Wu, Nanocarbon electrocatalysts for oxygen reduction in alkaline media for advanced energy conversion and storage, *Adv. Energy Mater.* 4 (2014), <http://dx.doi.org/10.1002/aenm.20130145>.

[18] H. Hou, G. Sun, R. He, B. Sun, W. Jin, H. Liu, Q. Xin, Alkali doped polybenzimidazole membrane for alkaline direct methanol fuel cell, *Int. J. Hydrogen Energy* 33 (2008) 7172–7176, <http://dx.doi.org/10.1016/j.ijhydene.2008.09.023>.

[19] H. Hou, G. Sun, R. He, Z. Wu, B. Sun, Alkali doped polybenzimidazole membrane for high performance alkaline direct ethanol fuel cell, *J. Power Sources* 182 (2008) 95–99, <http://dx.doi.org/10.1016/j.jpowsour.2008.04.010>.

[20] J.R. Varcoe, R.C.T. Slade, E.L.H. Yee, S.D. Poynton, D.J. Driscoll, Investigations into the ex situ methanol, ethanol and ethylene glycol permeabilities of alkaline polymer electrolyte membranes, *J. Power Sources* 173 (2007) 194–199, <http://dx.doi.org/10.1016/j.jpowsour.2007.04.068>.

[21] Z. Chen, D. Higgins, A. Yu, L. Zhang, J. Zhang, A review on non-precious metal electrocatalysts for PEM fuel cells, *Energy Environ. Sci.* 4 (2011) 3167–3192, <http://dx.doi.org/10.1039/c0ee00558d>.

[22] R. Othman, A.L. Dicks, Z. Zhu, Non precious metal catalysts for the PEM fuel cell cathode, *Int. J. Hydrogen Energy* 37 (2012) 357–372, <http://dx.doi.org/10.1016/j.ijhydene.2011.08.095>.

[23] H. Zhong, H. Zhang, S. Liu, C. Deng, M. Wang, Nitrogen-enriched carbon from melamine resins with superior oxygen reduction reaction activity, *ChemSusChem* 6 (2013) 807–812, <http://dx.doi.org/10.1002/cssc.201200919>.

[24] L. Osmieri, A.H.A. Monteverde Videla, M. Armandi, S. Specchia, Influence of different transition metals on the properties of Me-N-C (Me = Fe, Co, Cu, Zn) catalysts synthesized using SBA-15 as tubular nano-silica reactor for oxygen reduction reaction, *Int. J. Hydrogen Energy* 41 (2016) 22570–22588, <http://dx.doi.org/10.1016/j.ijhydene.2016.05.223>.

[25] L. Osmieri, A.H.A. Monteverde Videla, S. Specchia, Activity of Co-N multi walled carbon nanotubes electrocatalysts for oxygen reduction reaction in acid conditions, *J. Power Sources* 278 (2015) 296–307, <http://dx.doi.org/10.1016/j.jpowsour.2014.12.080>.

[26] L. Osmieri, A.H.A. Monteverde Videla, S. Specchia, Optimization of a Fe-N-C electrocatalyst supported on mesoporous carbon functionalized with polypyrrole for oxygen reduction reaction under both alkaline and acidic conditions, *Int. J. Hydrogen Energy* 41 (2016) 19610–19628, <http://dx.doi.org/10.1016/j.ijhydene.2016.05.270>.

[27] J. Burgess, R.I. Haines, Solubilities of 1,10-phenanthroline and substituted derivatives in water and in aqueous methanol, *J. Chem. Eng. Data* 23 (1978) 196–197.

[28] J. Tian, A. Morozan, M.T. Sougrati, M. Lefèvre, R. Chenitz, J.-P. Dodelet, D. Jones, F. Jaouen, Optimized synthesis of Fe/N/C cathode catalysts for PEM fuel cells: a matter of iron-ligand coordination strength, *Angew. Chem. Int. Ed. Engl.* 52 (2013) 6867–6870, <http://dx.doi.org/10.1002/anie.201303025>.

[29] M. Bron, J. Radnik, M. Fieber-Erdmann, P. Bogdanoff, S. Fiechter, EXAFS, XPS and electrochemical studies on oxygen reduction catalysts obtained by heat treatment of iron phenanthroline complexes supported on high surface area carbon black, *J. Electroanal. Chem.* 535 (2002) 113–119, [http://dx.doi.org/10.1016/S0022-0728\(02\)01189-0](http://dx.doi.org/10.1016/S0022-0728(02)01189-0).

[30] M. Lefèvre, E. Proietti, F. Jaouen, J.-P. Dodelet, Iron-based catalysts with improved oxygen reduction activity in polymer electrolyte fuel cells, *Science* 324 (2009) 71–74, <http://dx.doi.org/10.1126/science.1170051>.

[31] C.-W. Tsai, M.-H. Tu, C.-J. Chen, T.-F. Hung, R.-S. Liu, W.-R. Liu, M.-Y. Lo, Y.-M. Peng, L. Zhang, J. Zhang, D.-S. Shy, X.-K. Xing, Nitrogen-doped graphene nanosheet-supported non-precious iron nitride nanoparticles as an efficient electrocatalyst for oxygen reduction, *RSC Adv.* 1 (2011) 1349, <http://dx.doi.org/10.1039/c1ra00373a>.

[32] K. Strickland, E. Miner, Q. Jia, U. Tytus, N. Ramaswamy, W. Liang, M.-T. Sougrati, F. Jaouen, S. Mukerjee, Highly active oxygen reduction non-platinum group metal electrocatalyst without direct metal-nitrogen coordination, *Nat. Commun.* 6 (2015) 7343, <http://dx.doi.org/10.1038/ncomms8343>.

[33] U.I. Kramm, M. Lefèvre, N. Larouche, D. Schmeißer, J. Dodelet, Correlations between mass activity and physicochemical properties of Fe/N/C catalysts for the ORR in PEM fuel cell via 57 Fe Möbbauer spectroscopy and other techniques, *J. Am. Chem. Soc.* 136 (2014) 978–985.

[34] D. Zhao, J.-L. Shui, L.R. Grabstanowicz, C. Chen, S.M. Commet, T. Xu, J. Lu, D.-J. Liu, Highly efficient non-Precious metal electrocatalysts prepared from one-Pot synthesized zeolitic imidazolate frameworks, *Adv. Mater.* 26 (2014) 1093–1097, <http://dx.doi.org/10.1002/adma.201304238>.

[35] V. Armel, J. Hannauer, F. Jaouen, Effect of ZIF-8 crystal size on the O2 electro-Reduction performance of pyrolyzed Fe-N-C catalysts, *Catalysts* 5 (2015) 1333–1351, <http://dx.doi.org/10.3390/catal5031333>.

[36] F. Jaouen, F. Charreteur, J.P. Dodelet, Fe-Based catalysts for oxygen reduction in PEMFCs, *J. Electrochem. Soc.* 153 (2006) A689–A698.

[37] A.H.A. Monteverde Videla, L. Zhang, J. Kim, J. Zeng, C. Francia, J. Zhang, S. Specchia, Mesoporous carbons supported non-noble metal Fe-N-X electrocatalysts for PEM fuel cell oxygen reduction reaction, *J. Appl. Electrochem.* 43 (2013) 159–169, <http://dx.doi.org/10.1007/s10800-012-0497-y>.

[38] A. Santasalo-Aarnio, M. Borghei, I.V. Anoshkin, A.G. Nasibulin, E.I. Kauppinen, V. Ruiz, T. Kallio, Durability of different carbon nanomaterial supports with PtRu catalyst in a direct methanol fuel cell, *Int. J. Hydrogen Energy* 37 (2012) 3415–3424, <http://dx.doi.org/10.1016/j.ijhydene.2011.11.009>.

[39] C.W.B. Bezerra, L. Zhang, K. Lee, H. Liu, J. Zhang, Z. Shi, A.L.B. Marques, E.P. Marques, S. Wu, J. Zhang, Novel carbon-supported Fe-N electrocatalysts synthesized through heat treatment of iron tripyridyl triazine complexes for the PEM fuel cell oxygen reduction reaction, *Electrochim. Acta* 53 (2008) 7703–7710, <http://dx.doi.org/10.1016/j.electacta.2008.05.030>.

[40] D. Sebastián, A.G. Ruiz, I. Suelves, R. Moliner, M.J. Lázaro, V. Baglio, A. Stassi, A.S. Aricò, Enhanced oxygen reduction activity and durability of Pt catalysts supported on carbon nanofibers, *Appl. Catal. B Environ.* 115–116 (2012) 269–275, <http://dx.doi.org/10.1016/j.apcatb.2011.12.041>.

[41] E. Negro, A.H.A. Monteverde Videla, V. Baglio, A.S. Aricò, S. Specchia, G.J.M. Koper, Fe-N supported on graphitic carbon nano-networks grown from cobalt as oxygen reduction catalysts for low-temperature fuel cells, *Appl. Catal. B Environ.* 166–167 (2015) 75–83, <http://dx.doi.org/10.1016/j.apcatb.2014.10.074>.

[42] H.R. Byon, J. Suntivich, Y. Shao-Horn, Graphene-based non-noble-metal catalysts for oxygen reduction reaction in acid, *Chem. Mater.* 23 (2011) 3421–3428, <http://dx.doi.org/10.1021/cm2000649>.

[43] A.H.A. Monteverde Videla, S. Ban, S. Specchia, L. Zhang, J. Zhang, Non-noble Fe-NX electrocatalysts supported on the reduced graphene oxide for oxygen reduction reaction, *Carbon N. Y.* 76 (2014) 386–400, <http://dx.doi.org/10.1016/j.carbon.2014.04.092>.

[44] B. Zhang, Y. Xu, Y. Zheng, L. Dai, M. Zhang, J. Yang, Y. Chen, X. Chen, J. Zhou, A facile synthesis of polypyrrole/carbon nanotube composites with ultrathin, uniform and thickness-tunable polypyrrole shells, *Nanoscale Res. Lett.* 6 (2011) 431, <http://dx.doi.org/10.1186/1556-276X-6-431>.

[45] S. Shrestha, W.E. Mustain, Properties of nitrogen-Functionalized ordered mesoporous carbon prepared using polypyrrole precursor, *J. Electrochem. Soc.* 157 (2010) B1665, <http://dx.doi.org/10.1149/1.3489412>.

[46] J. Zeng, C. Francia, M. a. Dumitrescu, A.H. a. Monteverde Videla, V.S. Ijeri, S. Specchia, P. Spinelli, Electrochemical performance of Pt-based catalysts supported on different ordered mesoporous carbons (Pt/OMCs) for oxygen reduction reaction, *Ind. Eng. Chem. Res.* 51 (2012) 7500–7509, <http://dx.doi.org/10.1021/ie2016619>.

[47] F.J. Pérez-Alonso, M.A. Salam, T. Herranz, J.L. Gómez de la Fuente, S.A. Al-Thabaiti, S.N. Basahel, M. a. Peña, J.L.G. Fierro, S. Rojas, Effect of carbon nanotube diameter for the synthesis of Fe/N/multiwall carbon nanotubes and repercussions for the oxygen reduction reaction, *J. Power Sources* 240 (2013) 494–502, <http://dx.doi.org/10.1016/j.jpowsour.2013.04.086>.

[48] M. Ferrandon, A.J. Kropf, D.J. Myers, U. Kramm, P. Bogdanoff, G. Wu, C.M. Johnston, P. Zelenay, Multitechnique characterization of a polyaniline-iron-carbon oxygen reduction catalyst, *J. Phys. Chem. C* 116 (2012) 16001–16013.

[49] F. Jaouen, V. Goellner, M. Lefèvre, J. Herranz, E. Proietti, J.P. Dodelet, Oxygen reduction activities compared in rotating-disk electrode and proton exchange membrane fuel cells for highly active FeNC catalysts, *Electrochim. Acta* 87 (2013) 619–628, <http://dx.doi.org/10.1016/j.electacta.2012.09.057>.

[50] M. Montiel, S. García-Rodríguez, P. Hernández-Fernández, R. Díaz, S. Rojas, J.L.G. Fierro, E. Fatás, P. Ocón, Relevance of the synthesis route of Se-modified Ru/C as methanol tolerant electrocatalysts for the oxygen reduction reaction, *J. Power Sources* 195 (2010) 2478–2487, <http://dx.doi.org/10.1016/j.jpowsour.2009.11.080>.

[51] R. Escudero-Cid, J.C. Pérez-Flores, E. Fatás, P. Ocón, Degradation of DMFC using a new long-term stability cycle, *Int. J. Green Energy* 12 (2015) 641–653, <http://dx.doi.org/10.1080/15435075.2013.867269>.

[52] R. Escudero-Cid, P. Hernández-Fernández, J.C. Pérez-Flores, S. Rojas, S. García-Rodríguez, E. Fatás, P. Ocón, Analysis of performance losses of direct methanol fuel cell with methanol tolerant PtCoRu/C cathode electrode, *Int. J. Hydrogen Energy* 37 (2012) 7119–7130, <http://dx.doi.org/10.1016/j.ijhydene.2011.12.158>.

[53] S. Carrión-Satorre, M. Montiel, R. Escudero-Cid, J.L.G. Fierro, E. Fatás, P. Ocón, Performance of carbon-supported palladium and palladium-ruthenium catalysts for alkaline membrane direct ethanol fuel cells, *Int. J. Hydrogen*

Energy 41 (2016) 8954–8962, <http://dx.doi.org/10.1016/j.ijhydene.2016.04.053>.

[54] K.S.W. Sing, D.H. Everett, R.A.W. Haul, L. Moscou, R.A. Pierotti, J. Rouquerol, T. Siemieniewska, Reporting physisorption data for gas/solid systems with special reference to the determination of surface area and porosity, *Pure Appl. Chem.* 57 (1985) 603–619, <http://dx.doi.org/10.1351/pac198557040603>.

[55] M. Thommes, K. Kaneko, A.V. Neimark, J.P. Olivier, F. Rodriguez-Reinoso, J. Rouquerol, K.S.W. Sing, Physisorption of gases, with special reference to the evaluation of surface area and pore size distribution (IUPAC Technical Report), *Pure Appl. Chem.* (2015), <http://dx.doi.org/10.1515/pac-2014-1117>.

[56] Z. Li, Z. Pan, S. Dai, Nitrogen adsorption characterization of aligned multiwalled carbon nanotubes and their acid modification, *J. Colloid Interface Sci.* 277 (2004) 35–42, <http://dx.doi.org/10.1016/j.jcis.2004.05.024>.

[57] H. Sun, H. Su, X. Ma, P. Zhang, X. Zhang, X. Dai, J. Gao, C. Chen, S.-G. Sun, Fe/IRMOF-3 derived porous carbons as non-precious metal electrocatalysts with high activity and stability towards oxygen reduction reaction, *Electrochim. Acta* 205 (2016) 53–61, <http://dx.doi.org/10.1016/j.electacta.2016.04.037>.

[58] F. Jaouen, J. Herranz, M. Lefèvre, J.-P. Dodelet, U.I. Kramm, I. Herrmann, P. Bogdanoff, J. Maruyama, T. Nagaoka, A. Garsuch, J.R. Dahn, T. Olson, S. Pylypenko, P. Atanassov, E.a. Ustinov, Cross-laboratory experimental study of non-noble-metal electrocatalysts for the oxygen reduction reaction, *ACS Appl. Mater. Interfaces* 1 (2009) 1623–1639, <http://dx.doi.org/10.1021/am900219g>.

[59] A. Serov, K. Artyushkova, N.I. Andersen, S. Stariha, P. Atanassov, Original mechanochemical synthesis of non-platinum group metals oxygen reduction reaction catalysts assisted by sacrificial support method, *Electrochim. Acta* 179 (2015) 154–160, <http://dx.doi.org/10.1016/j.electacta.2015.02.108>.

[60] M.H. Robson, A. Serov, K. Artyushkova, P. Atanassov, A mechanistic study of 4-aminoantipyrine and iron derived non-platinum group metal catalyst on the oxygen reduction reaction, *Electrochim. Acta* 90 (2013) 656–665, <http://dx.doi.org/10.1016/j.electacta.2012.11.025>.

[61] P.H. Matter, L. Zhang, U.S. Ozkan, The role of nanostructure in nitrogen-containing carbon catalysts for the oxygen reduction reaction, *J. Catal.* 239 (2006) 83–96, <http://dx.doi.org/10.1016/j.jcat.2006.01.022>.

[62] J. Dodelet, *Electrocatalysis in Fuel Cells*, Springer London, London, 2013, <http://dx.doi.org/10.1007/978-1-4471-4911-8>.

[63] F. Jaouen, F. Charreteur, J.P. Dodelet, Fe-based catalysts for oxygen reduction in PEMFCs, *J. Electrochem. Soc.* 153 (2006) A689–A698, <http://dx.doi.org/10.1149/1.2168418>.

[64] Q. Liu, H. Zhang, H. Zhong, S. Zhang, S. Chen, N-doped graphene/carbon composite as non-precious metal electrocatalyst for oxygen reduction reaction, *Electrochim. Acta* 81 (2012) 313–320, <http://dx.doi.org/10.1016/j.electacta.2012.07.022>.

[65] M. Lezanska, P. Pietrzky, Z. Sojka, Investigations into the structure of nitrogen-containing CMK-3 and OCM-0.75 carbon replicas and the nature of surface functional groups by spectroscopic and sorption techniques, *J. Phys. Chem. C* 114 (2010) 1208–1216, <http://dx.doi.org/10.1021/jp909529x>.

[66] A. Ferrari, J. Robertson, Interpretation of Raman spectra of disordered and amorphous carbon, *Phys. Rev. B* 61 (2000) 14095–14107, <http://dx.doi.org/10.1103/PhysRevB.61.14095>.

[67] G. Wu, K.L. More, C.M. Johnston, P. Zelenay, High-performance electrocatalysts for oxygen reduction derived from polyaniline, iron, and cobalt, *Science* 332 (2011) 443–447, <http://dx.doi.org/10.1126/science.1200832>.

[68] N. Ramaswamy, S. Mukerjee, Fundamental mechanistic understanding of electrocatalysis of oxygen reduction on pt and non-Pt surfaces: acid versus alkaline media, *Adv. Phys. Chem.* 2012 (2012) 1–17, <http://dx.doi.org/10.1155/2012/491604>.

[69] S.L. Gojković, S. Gupta, R.F. Savinell, Heat-treated iron(III) tetramethoxyphenyl porphyrin chloride supported on high-area carbon as an electrocatalyst for oxygen reduction: part III. Detection of hydrogen-peroxide during oxygen reduction, *Electrochim. Acta* 45 (1999) 889–897, [http://dx.doi.org/10.1016/S0013-4686\(99\)00294-7](http://dx.doi.org/10.1016/S0013-4686(99)00294-7).

[70] J. Masa, C. Batchelor-McAuley, W. Schuhmann, R.G. Compton, Koutecky-Levich analysis applied to nanoparticle modified rotating disk electrodes: electrocatalysis or misinterpretation, *Nano Res.* 7 (2013) 71–78, <http://dx.doi.org/10.1007/s12274-013-0372-0>.

[71] K. Kinoshita, *Carbon: Electrochemical and Physicochemical Properties*, Wiley Interscience, New York, NY, 1988.

[72] N. Ramaswamy, S. Mukerjee, Influence of inner- and outer-sphere electron transfer mechanisms during electrocatalysis of oxygen reduction in alkaline media, *J. Phys. Chem. C* 115 (2011) 18015–18026, <http://dx.doi.org/10.1021/jp204680p>.

[73] M. Zhani, H.A. Gasteiger, M. Piana, S. Catanorchi, Comparative study between platinum supported on carbon and non-noble metal cathode catalyst in alkaline direct ethanol fuel cell (ADEFC), *Int. J. Hydrogen Energy* 36 (2011) 5110–5116, <http://dx.doi.org/10.1016/j.ijhydene.2011.01.079>.

[74] U.A. Paulus, T.J. Schmidt, H.A. Gasteiger, R.J. Behm, Oxygen reduction on a high-surface area Pt/Vulcan carbon catalyst: a thin-film rotating ring-disk electrode study, *J. Electroanal. Chem.* 495 (2001) 134–145, [http://dx.doi.org/10.1016/S0022-0728\(00\)00407-1](http://dx.doi.org/10.1016/S0022-0728(00)00407-1).

[75] N.M. Markovic, T.J. Schmidt, V. Stamenkovic, P.N. Ross, Oxygen reduction reaction on pt and Pt bimetallic surfaces: a selective review, *Fuel Cells* 1 (2001) 105–116, [http://dx.doi.org/10.1002/1615-6854\(200107\)1:2<105::aid-fuce105>3.0.co;2-0](http://dx.doi.org/10.1002/1615-6854(200107)1:2<105::aid-fuce105>3.0.co;2-0).

[76] I.A. Pasti, N.M. Gavrilov, S.V. Mentus, Potentiodynamic investigation of oxygen reduction reaction on polycrystalline platinum surface in acidic solutions: the effect of the polarization rate on the kinetic parameters, *Int. J. Electrochem. Sci.* 7 (2012) 11076–11090.

[77] G. Zhang, R. Chenitz, M. Lefèvre, S. Sun, J.P. Dodelet, Is iron involved in the lack of stability of Fe/N/C electrocatalysts used to reduce oxygen at the cathode of PEM fuel cells? *Nano Energy* (2016) 1–15, <http://dx.doi.org/10.1016/j.nanoen.2016.02.038>.

[78] R. Escudero-Cid, M. Montiel, L. Sotomayor, B. Loureiro, E. Fatás, P. Ocón, Evaluation of polyaniline-naion® composite membranes for direct methanol fuel cells durability tests, *Int. J. Hydrogen Energy* 40 (2015) 8182–8192, <http://dx.doi.org/10.1016/j.ijhydene.2015.04.130>.

[79] D. Sebastián, A. Serov, K. Artyushkova, J. Gordon, P. Atanassov, A.S. Aricò, V. Baglio, High performance and cost-Effective direct methanol fuel cells: Fe-N-C methanol-tolerant oxygen reduction reaction catalysts, *ChemSusChem* 9 (2016) 1986–1995, <http://dx.doi.org/10.1002/cssc.201600583>.

[80] N.S. Vasile, R. Doherty, A.H.A. Monteverde Videla, S. Specchia, 3D multi-physics modeling of a gas diffusion electrode for oxygen reduction reaction for electrochemical energy conversion in PEM fuel cells, *Appl. Energy* 175 (2016) 435–450, <http://dx.doi.org/10.1016/j.apenergy.2016.04.030>.

[81] A.H.A. Monteverde Videla, D. Sebastian, N.S. Vasile, L. Osmieri, A.S. Aricò, V. Baglio, S. Specchia, Performance analysis of Fe-N-C catalyst for DMFC cathodes: effect of water saturation in the cathodic catalyst layer, *Int. J. Hydrogen Energy* 41 (2016) 22605–22618, <http://dx.doi.org/10.1016/j.ijhydene.2016.06.060>.

[82] D. Sebastián, A. Serov, K. Artyushkova, P. Atanassov, A.S. Aricò, V. Baglio, Performance, methanol tolerance and stability of Fe-aminobenzimidazole derived catalyst for direct methanol fuel cells, *J. Power Sources* 319 (2016) 235–246, <http://dx.doi.org/10.1016/j.jpowsour.2016.04.067>.

[83] B. Piela, T.S. Olson, P. Atanassov, P. Zelenay, Highly methanol-tolerant non-precious metal cathode catalysts for direct methanol fuel cell, *Electrochim. Acta* 55 (2010) 7615–7621, <http://dx.doi.org/10.1016/j.electacta.2009.11.085>.

[84] Q. He, T. Mugadza, G. Hwang, T. Nyokong, Mechanisms of electrocatalysis of oxygen reduction by metal porphyrins in trifluoromethane sulfonic acid solution, *Int. J. Electrochem. Sci.* 7 (2012) 7045–7064.

[85] C.H. Choi, C. Baldizzone, G. Polymeros, E. Pizzutilo, O. Kasian, A.K. Schuppert, N. Ranjbar Sahraie, M.-T. Sougrati, K.J.J. Mayrhofer, F. Jaouen, Minimizing operando demetallation of Fe-N-C electrocatalysts in acidic medium, *ACS Catal.* (2016) 3136–3146, <http://dx.doi.org/10.1021/acscatal.6b00643>.

[86] G. Liu, X. Li, P. Ganeshan, B.N. Popov, Studies of oxygen reduction reaction active sites and stability of nitrogen-modified carbon composite catalysts for PEM fuel cells, *Electrochim. Acta* 55 (2010) 2853–2858, <http://dx.doi.org/10.1016/j.electacta.2009.12.055>.

[87] M. Lefèvre, J.-P. Dodelet, Fe-based catalysts for the reduction of oxygen in polymer electrolyte membrane fuel cell conditions: determination of the amount of peroxide released during electroreduction and its influence on the stability of the catalysts, *Electrochim. Acta* 48 (2003) 2749–2760, [http://dx.doi.org/10.1016/S0013-4686\(03\)00393-1](http://dx.doi.org/10.1016/S0013-4686(03)00393-1).

[88] V. Goellner, V. Armel, A. Zitolo, E. Fonda, F. Jaouen, Degradation by hydrogen peroxide of metal-nitrogen-carbon catalysts for oxygen reduction, *J. Electrochem. Soc.* 162 (2015) H403–H414, <http://dx.doi.org/10.1149/2.1091506jes>.

[89] L.G. Bloor, P.J. Molina, M.D. Symes, L. Cronin, Low pH electrolytic water splitting using earth-abundant metastable catalysts that self-assemble in situ, *J. Am. Chem. Soc.* 136 (2014) 3304–3311, <http://dx.doi.org/10.1021/ja5003197>.

[90] R. Krishna, Describing the diffusion of guest molecules inside porous structures, *J. Phys. Chem. C* 113 (2009) 19756–19781, <http://dx.doi.org/10.1021/jp906879d>.

[91] A. Grosman, C. Ortega, Nature of capillary condensation and evaporation processes in ordered porous materials, *Langmuir* 21 (2005) 10515–10521, <http://dx.doi.org/10.1021/la051030a>.

[92] F. Jaouen, M. Lefèvre, J.-P. Dodelet, M. Cai, Heat-treated Fe/N/C catalysts for O₂ electroreduction: are active sites hosted in micropores? *J. Phys. Chem. B* 110 (2006) 5553–5558, <http://dx.doi.org/10.1021/jp057135h>.

[93] Y.S. Li, T.S. Zhao, Z.X. Liang, Performance of alkaline electrolyte-membrane-based direct ethanol fuel cells, *J. Power Sources* 187 (2009) 387–392, <http://dx.doi.org/10.1016/j.jpowsour.2008.10.132>.

[94] H. Li, Y. Tang, Z. Wang, Z. Shi, S. Wu, D. Song, J. Zhang, K. Fatih, J. Zhang, H. Wang, Z. Liu, R. Abouatallah, A. Mazza, A review of water flooding issues in the proton exchange membrane fuel cell, *J. Power Sources* 178 (2008) 103–117, <http://dx.doi.org/10.1016/j.jpowsour.2007.12.068>.

[95] Y.S. Li, T.S. Zhao, R. Chen, Cathode flooding behaviour in alkaline direct ethanol fuel cells, *J. Power Sources* 196 (2011) 133–139, <http://dx.doi.org/10.1016/j.jpowsour.2010.06.111>.

[96] A.C. Garcia, J.J. Linares, M. Chatenet, E.a. Ticianelli, NiMnO_x/C: a non-noble ethanol-tolerant catalyst for oxygen reduction in alkaline exchange membrane DEFC, *Electrocatalysis* 5 (2013) 41–49, <http://dx.doi.org/10.1007/s12678-013-0162-1>.

[97] Y.S. Li, T.S. Zhao, Z.X. Liang, Effect of polymer binders in anode catalyst layer on performance of alkaline direct ethanol fuel cells, *J. Power Sources* 190 (2009) 223–229, <http://dx.doi.org/10.1016/j.jpowsour.2009.01.055>.

[98] S.D. Poynton, R.C.T. Slade, T.J. Omasta, W.E. Mustain, R. Escudero-Cid, P. Ocón, J.R. Varcoe, Preparation of radiation-grafted powders for use as anion exchange ionomers in alkaline polymer electrolyte fuel cells, *J. Mater. Chem. A* 2 (2014) 5124, <http://dx.doi.org/10.1039/c4ta00558a>.

[99] L. Wang, E. Magliocca, E.L. Cunningham, W.E. Mustain, S.D. Poynton, R. Escudero-Cid, M.M. Nasef, J. Ponce-González, R. Bance-Souahli, R.C.T. Slade, D.K. Whelligan, J.R. Varcoe, An optimised synthesis of high performance radiation-grafted anion-exchange membranes, *Green Chem.* (2017), <http://dx.doi.org/10.1039/c6gc02526a>.

[100] H. Hou, S. Wang, Q. Jiang, W. Jin, L. Jiang, G. Sun, Durability study of KOH doped polybenzimidazole membrane for air-breathing alkaline direct ethanol fuel cell, *J. Power Sources* 196 (2011) 3244–3248, <http://dx.doi.org/10.1016/j.jpowsour.2010.11.104>.